1221

LEACH CORPORATION
CONTROLS DIVISION

ENGINEERING TEST REPORT

FINAL REPORT
FOR
ENDLESS LOOP RECORDER SERVO
CONTROL UNIT

GPO PRICE $
CFSTI PRICE(S) $
Hard copy (HC)
Microfiche (MF)
ff 653 July 65

Date: December 12, 1967	Job Number: 812102	Report Number: 23
Customer: NASA Goddard		
Project:		
Prepared By: E. A. Cooper		
Approved By: R. D. Petit		Page ____ of ____

FINAL REPORT

FOR

ENDLESS LOOP RECORDER SERVO CONTROL UNIT

CONTRACT NO. NAS 5-9445

Prepared By

LEACH CORPORATION, CONTROLS DIVISION
717 North Coney Avenue
Azusa, California

12 December 1967

Prepared For

GODDARD SPACE FLIGHT CENTER
Greenbelt, Maryland

FINAL REPORT

FOR

ENDLESS LOOP RECORDER SERVO CONTROL UNIT

CONTRACT NO. NAS 5-9445

Prepared By

LEACH CORPORATION, CONTROLS DIVISION
717 North Coney Avenue
Azusa, California

12 December 1967

Prepared For

GODDARD SPACE FLIGHT CENTER
Greenbelt, Maryland

Approved By: 

R. W. Wells, Manager of Engineering

SUMMARY

A study leading to a brushless DC motor servo used in conjunction with a dejittering buffer has been completed. The study was conducted on an endless loop recorder intended for space applications where minimum power, weight, size, and maximum reliability are paramount considerations.

An open loop tape drive system, utilizing a hysteresis AC motor, was found to be satisfactory for the record mode of operation, thereby eliminating the need for a tone wheel or similar device as a part of system requirements. It is recognized, however, that a single BDCM used in conjunction with a clutch, or the use of a second BDCM, would be appropriate alternative approaches. The choice of the three alternatives must be weighted by overall system size, weight, power and cost requirements.

Using a phase-locked servo technique in the playback mode, a servo bandwidth of 70 Hz was achieved. Analysis of the tape flutter spectrum above 70 Hz during closed loop operation of the servo led to determination of size requirements for a dejittering buffer. The buffer, used to effectively remove the jitter components left uncompensated by the servo, has a data capacity of 8 bits. The total servo system is packaged in 32.5 in^3 volume weighing 15 ounces and operates on 1.5 watts average and 4.0 watts peak power.

The combined compensation techniques will enable the data to be clocked out of a space vehicle recorder with a crystal or other stable oscillator, thereby eliminating time base error (jitter) normally encountered with a tape recorder. Greatly improved data accuracies, more optimum transition densities, and improved transmission signal-to-noise ratio can be achieved by this method.

TABLE OF CONTENTS

SECTION	TITLE	PAGE
	Summary	iii
	Table of Contents	iv
	List of Illustrations	v
	List of Tables	vi
1.0	Introduction	1
1.1	Aim	1
1.2	Scope	1
2.0	Discussion	2
2.1	Error Analyses	2
2.2	Brushless DC Motor Characteristics	4
2.3	Servo System Design Criteria	7
2.4	Servo System Description	7
2.5	Circuit Description and Analysis	11
2.6	Servo System Analysis	26
2.7	Servo System Performance	33
3.0	Conclusions	40
Appendix I	Eccentricity Analysis	42
Appendix II	Transmissibility Analysis	45
Appendix III	Reference Oscillator Analysis	49

LIST OF ILLUSTRATIONS

FIGURE NO.	TITLE	PAGE
1	Drive System Diagram	3
2	BDCM Functional Flow Diagram	6
3	Motor Torque Versus Position	8
4	Transport Reproduce Servo Functional Schematic	9
5	Servo System Block Diagram	10
6	Servo Amplifier Block Diagram	12
7	Phase Detector Schematic Diagram	14
8	Phase Detector State Variable Diagram	15
9	RC Filter Network	16
10	Control Amplifier Schematic	18
11	Integrated Circuit Amplifier	19
12	Compensation Circuit Schematic	20
13	Bode Diagram for Minor Loop	21
14	Reference Oscillator Schematic	22
15	BIØC, NRZC, and Clock	24
16	Data Converter and Clock Generator Block Diagram	25
17	Dejittering Buffer Block Diagram	27
18	Buffer Timing Diagram, 8 Bit	28
19	Closed Loop Transfer Function	29
20	Tracking Error Coefficient	31
21	Inverse Stiffness Plot	32
22	Unit Step Response	34
23	Open Loop Tape Flutter Frequency Spectrum	36
24	Open Loop Time Base Error (Accumulative Bit Jitter) Frequency Spectrum	37
25	Closed Loop Time Base Error (Accumulative Bit Jitter) Frequency Spectrum	39
26	System Assembly	41
AI-1	Diagram of Eccentricity	43
AII-1	Simple Belt Drive System	46

LIST OF TABLES

TABLE NO.	TITLE	PAGE
I	Flutter Due To Eccentricity	2
II	Transport Natural Frequencies	4

1.0 INTRODUCTION

1.1 AIM

It is the aim of this report to present the results of a detailed study and developmental effort under Contract No. NAS 5-9445 for a servo control unit to be used on an endless loop magnetic tape recorder.

Pursuant to the above contract and NASA GSFC Developmental Specification for Endless Loop Magnetic Tape Recorder Servo Control Unit, dated 3 August 1966, the study was conducted utilizing a NASA furnished endless loop tape transport, Model 489, Serial No. 2. The transport, intended for use in the storage of a single track of digital data in satellite applications, consisted of an inside/outside, endless loop tape pack, mechanical drive train, an AC hysteresis motor for record mode tape drive, and a Herbert C. Rotors brushless DC motor, Serial No. 5, for reproduce mode tape drive. Based upon the study results, a prototype servo package has been designed, built, and evaluated.

1.2 SCOPE

The scope of the study program, and hence the embodiment of this report, includes the necessary electrical and physical analysis to predict servo requirements and empirical testing to verify the predictions. The results of analysis and testing lead to an optimal servo control unit which contains: 1) closed loop tape speed control, 2) circuitry for the conversion of bi-phase change data (also known as Manchester coded) to NRZC data and the generation of a tape clock signal, and 3) data buffering circuitry for the purposes of dejittering.

2.0 DISCUSSION

2.1 ERROR ANALYSES

The major dynamic error sources of a transport result from the non-ideal character of the drive motors and the speed transformation drive system.

2.1.1 Eccentricity

Eccentricity of drive shafts is a source of tape jitter. A derivation of the equations describing tape position error due to shaft eccentricity is included in Appendix I. Table I gives the flutter characteristics due to eccentricity of the furnished transport. A definition of terms for the assembly is provided by Figure 1.

TABLE I
FLUTTER DUE TO ECCENTRICITY

	Percent Eccentricity (e/r)	Record Mode		Playback Mode	
		Percent Flutter	Flutter Freq.(Hz)	Percent Flutter	Flutter Freq.(Hz)
Record Motor Shaft	0.03	.03	32.4	.03	820
Idler Pulley	0.01	.01	2.4	.01	60.5
Idler Shaft	0.32	.32	2.4	.32	60.5
Output Capstan Pulley	0.01	.01	0.227	.01	5.79
Output Capstan Coupling Pulley	0.03	.03	0.227	.03	5.79
Output Capstan Shaft	0.00	---	0.227	---	5.79
Playback Motor Pulley	0.06	NA	NA	.06	33.3
Input Capstan Pulley	0.00	---	---	---	5.68
Input Capstan Coupling Pulley	0.00	---	---	---	5.68
Input Capstan Shaft	0.00	---	---	---	5.68

It is noteworthy that for the unit tested the flutter contribution due to eccentricity is negligibly small.

2.1.2 Transmissibility

The design of high performance servos typically requires the consideration of mechanical parasities. The bandwidth limitations of a belt coupled transmission system may be described in terms of the transfer function relating the shaft angles

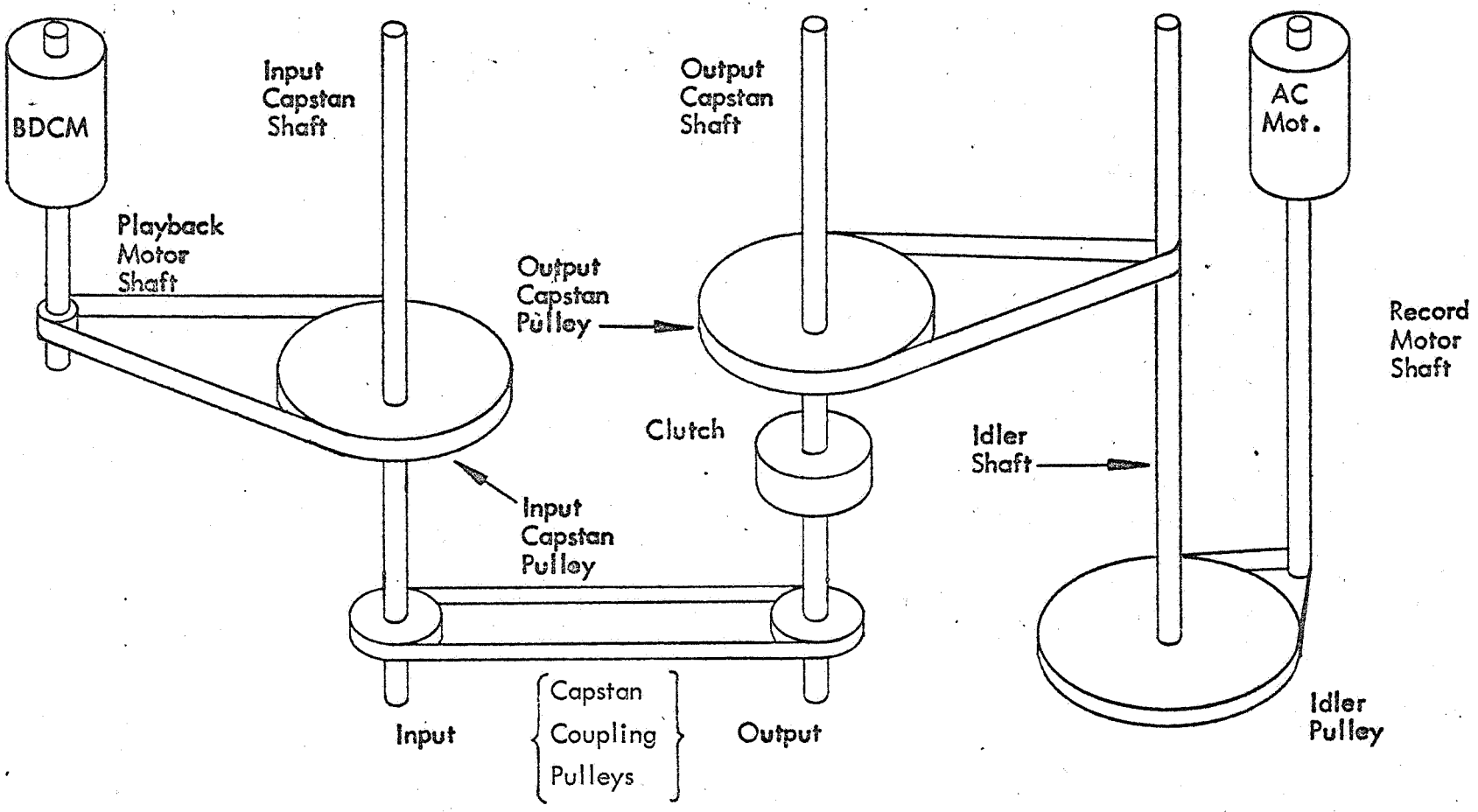

DRIVE SYSTEM DIAGRAM

FIGURE 1

of a two shaft assembly. This transfer function is defined as the transmissibility of the shaft pair. A general treatment of transmissibility is included in Appendix II. The poles of the transmissibility equations are the natural frequencies of transport drive system. Table II gives the natural frequencies derived for the furnished transport.

TABLE II
TRANSPORT NATURAL FREQUENCIES

	Effective Inertia J_T in^2 oz^2	Effective Spring Constant in/oz/rad	Natural Freq. w_n Hz
Record Motor - Idler	.615	2560	200
Idler - Capstan	.24	2134	295
Capstan-Capstan (Record)	5.4	190	18.5
Capstan-Capstan (Playback)	.005	190	610
Playback Motor - Capstan	.24	1067	208
Pinch Roller Arm	.787	215	54
Reel - Capstan	2.6	432	40

Qualification of the values in Table II must be made. Evaluation of inertia and spring constants involved simplifying idealizations. The findings serve to characterize resonances qualitatively and aid in interpretation of the flutter spectrum measured.

2.2 BRUSHLESS DC MOTOR CHARACTERISTICS

Information concerning the mechanization of the brushless DC motor was obtained from the Herbert C. Rotors data and NASA Technical Note, NASA TN D-2819 by Phillip A. Studer, along with considerable empirically derived data. Resultant measured parameters follow:

Electrical:

R = resistance = 135 ohms

L = inductance = .05 henrys

Electromechanical:

K_t = torque constant = 5.85 $\frac{\text{oz-in}}{\text{amp}}$

K_v = back emf constant = 0.056 $\frac{\text{volts}}{\text{rad/sec}}$

Mechanical:

J = rotor inertia = 0.55×10^{-4} oz-in-sec^2

T_f = Coulomb friction = 0.03 oz-in

The characteristic equations for a DC motor are:

$$V = iR + L\frac{di}{dt} + K_v\frac{d\theta}{dt}$$

$$K_t i = J\frac{d^2\theta}{dt^2} + T_f S_{gn}\frac{d\theta}{dt}$$

Where V is voltage at the motor terminals, θ is rotor angle, and windage is neglected. For the application at hand, T_f is constant and may be ignored for transfer analysis purposes.

Using Laplace Transform notation and solving the above equations simultaneously yields:

$$\frac{\theta(S)}{V(S)} = \frac{1/K_v}{S\left(\frac{JL}{K_v K_t}S^2 + \frac{JR}{K_v K_t}S + 1\right)}$$

The resultant expression is described schematically in Figure 2.

For the parameters measured, the motor transfer function is:

$$\frac{\theta(S)}{V(S)} = \frac{1/.056\frac{\text{rad}}{\text{volt}}}{S\,(.00038\,S + 1)\,(.021\,S + 1)}$$

If motor current is the control variable, the motor transfer function is:

$$\frac{\theta(S)}{I(S)} = \frac{1.06 \times 10^5}{S^2}\ \frac{\text{rad}}{\text{amp}}$$

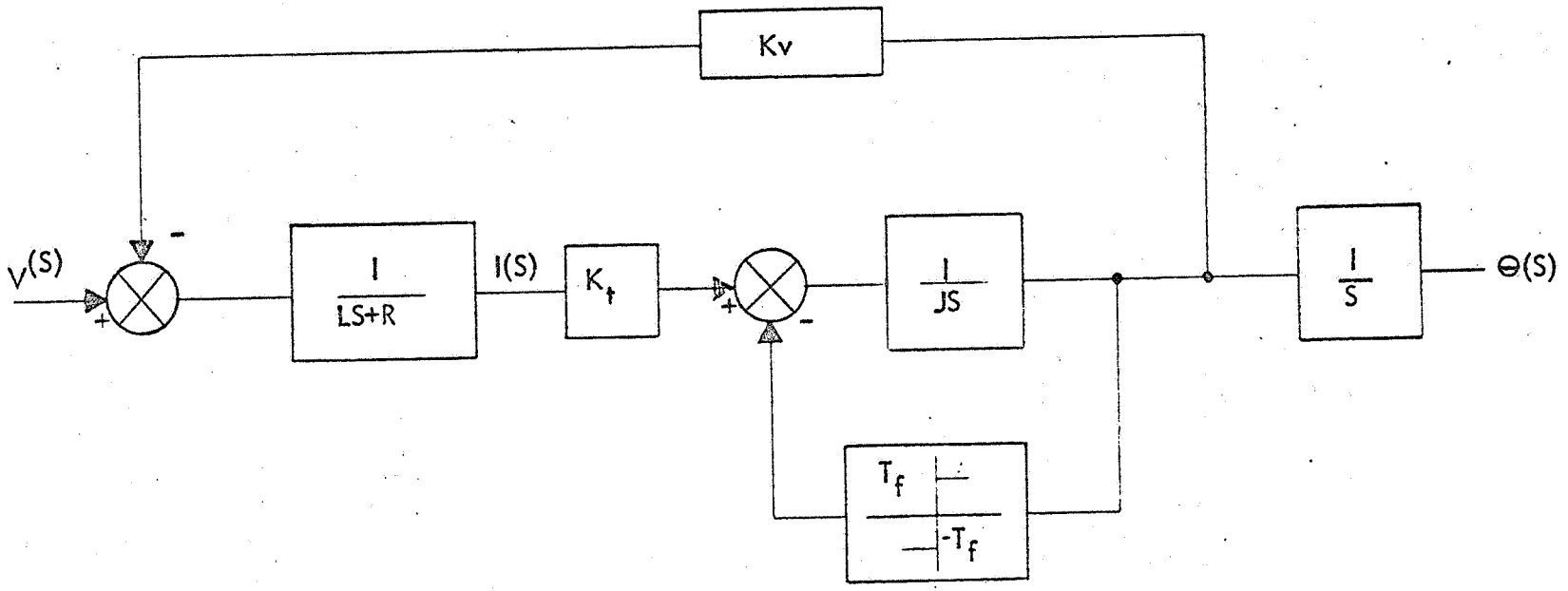

BDCM FUNCTIONAL FLOW DIAGRAM

FIGURE 2

Due to commutation and slot effects, ripple torque; i.e., periodic variation of torque output with rotor position is an intrinsic error of a DC motor. Measured torque output as a function of rotor position is shown in Figure 3. Twenty percent ripple was measured and occurs at a twenty times per revolution rate. The current level used for test is the steady-state current level measured during closed loop operation.

2.3 SERVO SYSTEM DESIGN CRITERIA

The main design criterion for a digital data tape transport servo is to reduce tape jitter to less than one-half a data bit width (peak). Ideally, this requirement could be met by extending the servo bandwidth beyond the highest significant error frequency. In practice, however, servo bandwidth is limited by high-order effects such as transport natural frequencies, noise-limiting, and torque limiting. Jitter resulting from error terms beyond the servo bandwidth can be removed by a dejittering buffer or data servo. Since the storage capacity requirements of a dejittering buffer are directly proportional to the magnitude of uncompensated jitter, it is desirable to remove as much jitter as possible with a tape servo.

Results from the analysis of transport characteristics predict a motor to capstan resonance of 200 Hz during playback. The spectral analysis of tape flutter given in Figure 24 shows a significant 180-200 Hz term. The behavior of the breadboard servo shows that the servo bandwidth cannot be extended beyond 100 Hz without a 200 Hz oscillation saturating the loop. Since this resonance characteristic is interior to the playback servo (see Figure 4), the transport becomes a fourth order system at 200 Hz. The torque requirements, the unpredictability of the resonance characteristics, and wear effects of exciting resonance make it impractical to attempt to servo at or beyond this natural frequency. A servo bandwidth of 70 Hz is considered to be a safe limit.

2.4 SERVO SYSTEM DESCRIPTION

The servo system is detailed in Figure 5. The system is type two (2); that is, position controlled with zero steady-state velocity error. Tape position is sensed by decoding a tape clock signal from any data recorded on the tape. The tape clock is phase compared with a reference oscillator signal. The phase error signal is compensated and amplified by the control amplifier which drives a brushless DC motor. The motor drives the differential capstan assembly through a pulley reduction system.

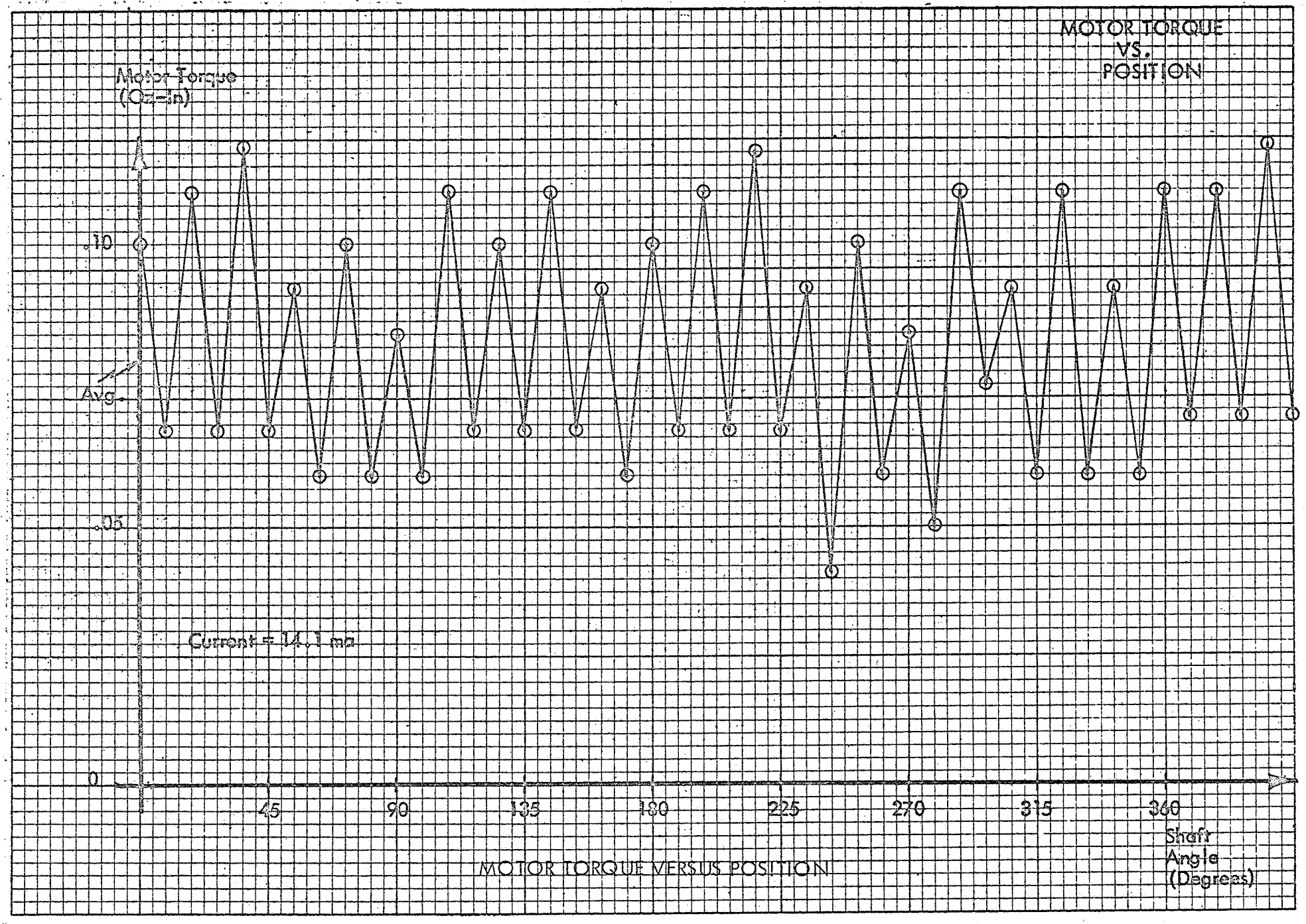

FIGURE 3

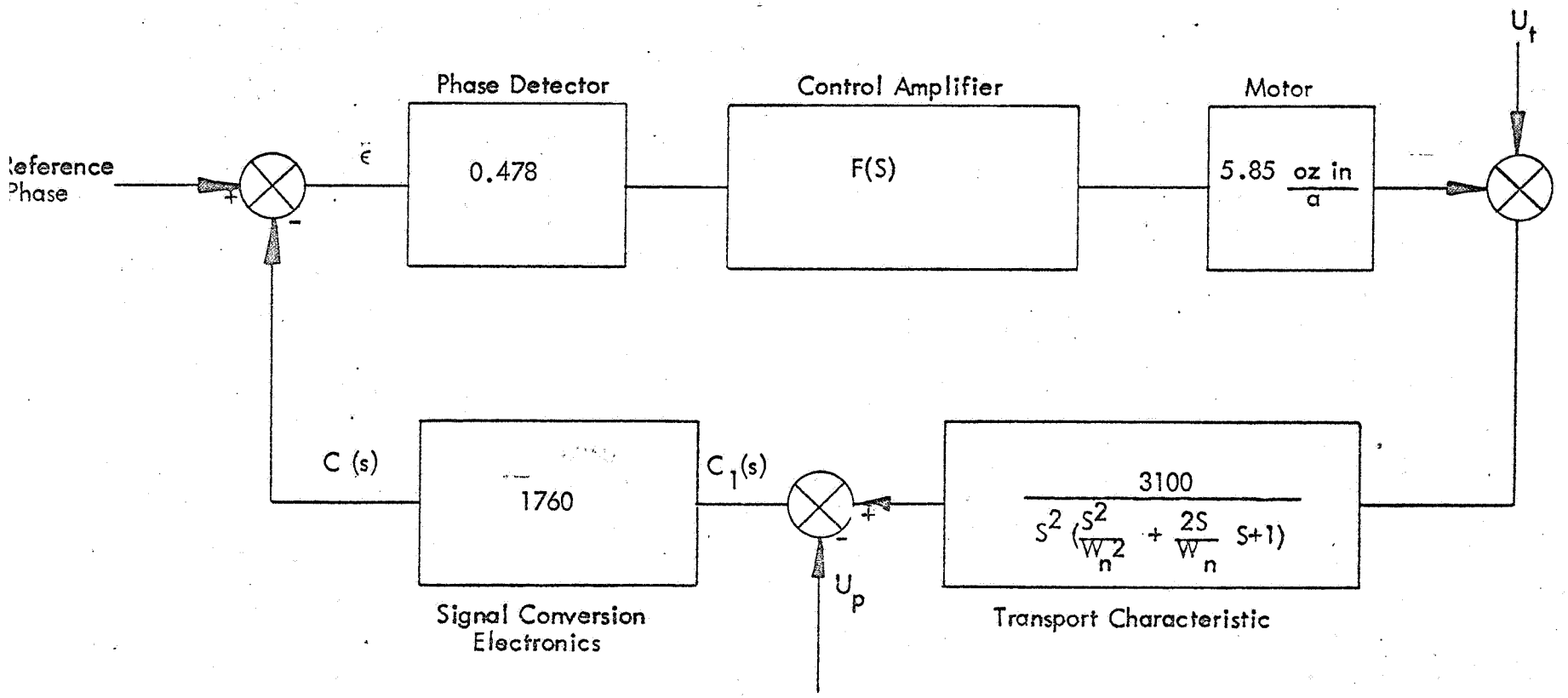

Where

$$F(S) = \frac{.0167\,(.071\,S + 1)\,(.01\,S + 1)}{(4.8\,S + 1)\,(.001\,S + 1)\,(.00022\,S + 1)\,(.00016S+1)}$$

U_p = Position error command

U_t = Torque disturbance

TRANSPORT REPRODUCE SERVO FUNCTIONAL SCHEMATIC

FIGURE 4

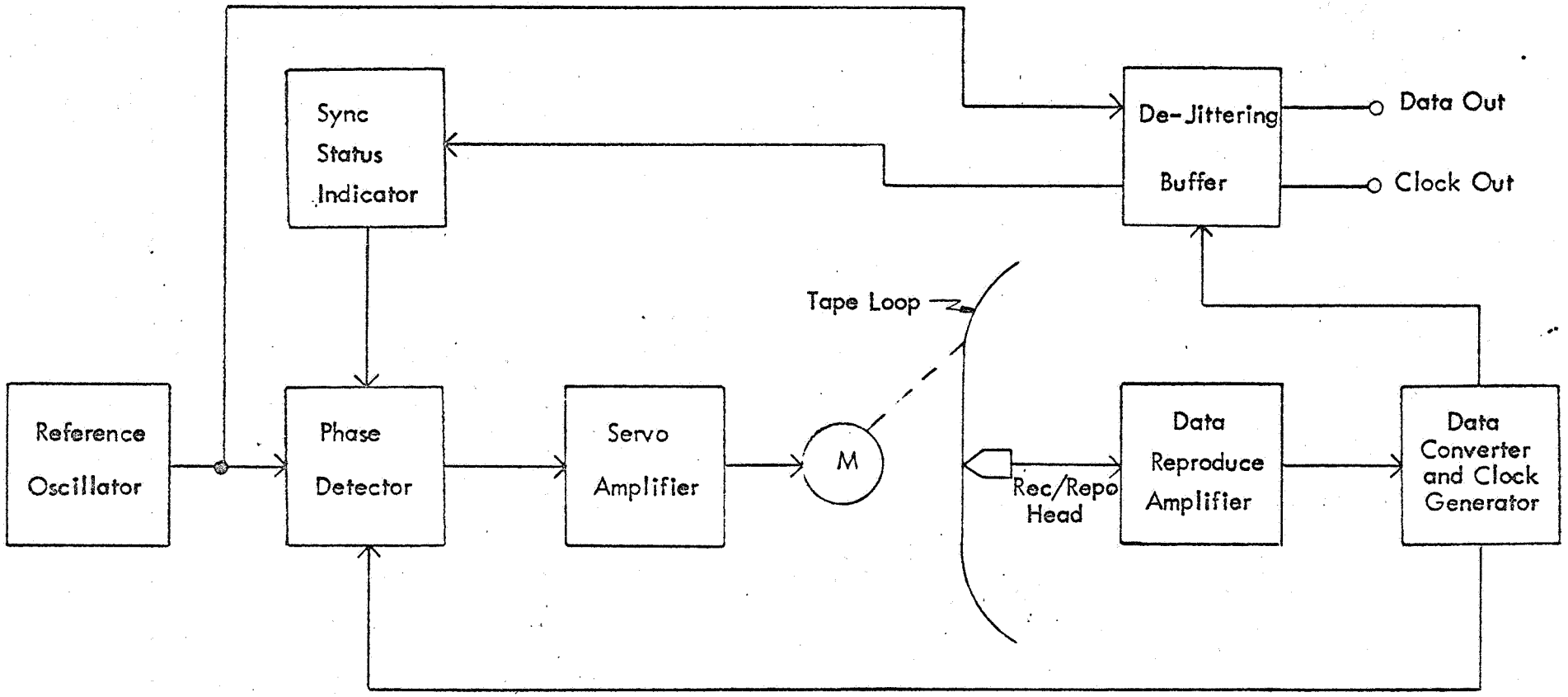

SERVO SYSTEM BLOCK DIAGRAM

FIGURE 52

An eight bit buffer is used to completely dejitter playback data. Under nominal conditions, the loading cell of the buffer is four bits removed from the unloading cell. For this condition a maximum time base error of three bits may be withstood.

In order to prevent relative drift of the load and unload points in the buffer and thereby assure maximum buffer capacity during transients, a second control signal is employed. The relative position of the buffer load and unload points is sensed once every eight bits by the buffer status detector. If the relative position is in error by more than one bit, an appropriate clock pulse is deleted from the inputs to the phase comparator in the control amplifier. The phase error produced is that required to shift the tape position one bit. As described, this second control loop affects the servo behavior only when data jitter into the buffer exceeds one bit. The one bit dead zone is appropriate for this system because the phase comparator has a linear range of one bit and will account for one bit position errors by the logical phase comparison.

An AC motor was used for the record mode and the brushless DC motor for the playback mode. Both motors were operated at 2,000 RPM with the appropriate speed reduction between each motor and the capstan to achieve the tape speed specified above. The motor supplying the capstan drive was coupled through a clutch arrangement which provided a disconnect of the AC record motor while in the playback mode. This concept allows operation of both motors at their most efficient speed, thereby optimizing performance and improving reliability.

2.5 CIRCUIT DESCRIPTION AND ANALYSIS

2.5.1 Servo Amplifier

The servo amplifier consists of a digital phase comparator which algebraically sums and demodulates two FM pulse trains and a high gain integrated circuit amplifier, operating in conjunction with a voltage isolation and power amplification stage necessary for compatible operation with the DC brushless motor. Signal compensation is employed by using motor current as a feedback signal operating through an RC compensation network. In this way the overall servo transfer function is made insensitive to the motor electrical break frequency. In addition, this operational style of compensation yields a high DC gain resulting in an overall servo error insensitivity to steady-state torque variations. Figure 6 shows the functional form of the servo amplifier.

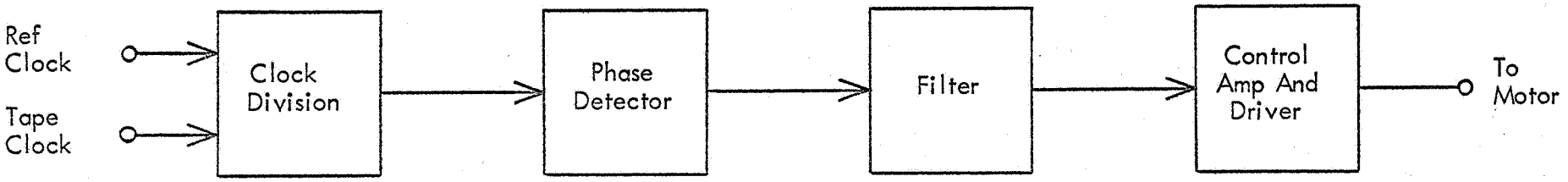

SERVO AMPLIFIER BLOCK DIAGRAM

Figure 6

Multiple minor loop feedback is used to stabilize the integrated circuit amplifier, as well as achieve the control amplifier transfer function required for servo system stability. For circuit analysis purposes, the servo amplifier may be divided into three sections which may be analyzed independently. These sections are the phase detector, the RC filter network, and the control amplifier section.

The phase detector is essentially an up-down counter with four stable sequential states. The circuit is shown in Figure 7. The state diagram for the counter is shown in Figure 8. The inputs are the reference clock square wave and the tape clock pulse train decoded from tape data. The input signals are divided by two in order to reduce the weighting function of the device, thereby assuring an unsaturated output signal under normal steady-state error conditions. The output is the center bit value of the counter. The output signal is a variable duty cycle square wave with an average value proportional to the phase difference of the input signals. The peak-to-peak linear range of the circuit is seen to be 4 π radians phase error between the input signals, however, the mnemonic capacity of the phase detector is 8 π radians. Since the maximum output signal is the supply voltage V_{cc}, the phase detector transfer function is $V_{cc}/4\ \pi$ volts per radian.

The RC filter network is shown in Figure 9. Note that R3 does not terminate at ground in the total control amplifier circuit, but is assumed to do so here because R3 functions as the input resistor of an operational amplifier.

Nodal analysis of the circuit yields a transfer function

$$\frac{e_0}{e_1} = \frac{1}{R1\ C1\ R2\ C2\ S^2 + (R1\ C1 + R1\ C2 + R2\ C1 + \frac{R1\ R2\ C2}{R3})\ S + 1 + \frac{R2 + R1}{R3}}$$

The circuit values chosen are

$$R1 = R2 = R3 = 43K$$
$$C1 = .033\ \mu f$$
$$C2 = .0082\ \mu f$$

Substituting values, the filter transfer function is

$$K_f\ (S) = \frac{.33}{(.001\ S + 1)\ (.00016\ S + 1)}$$

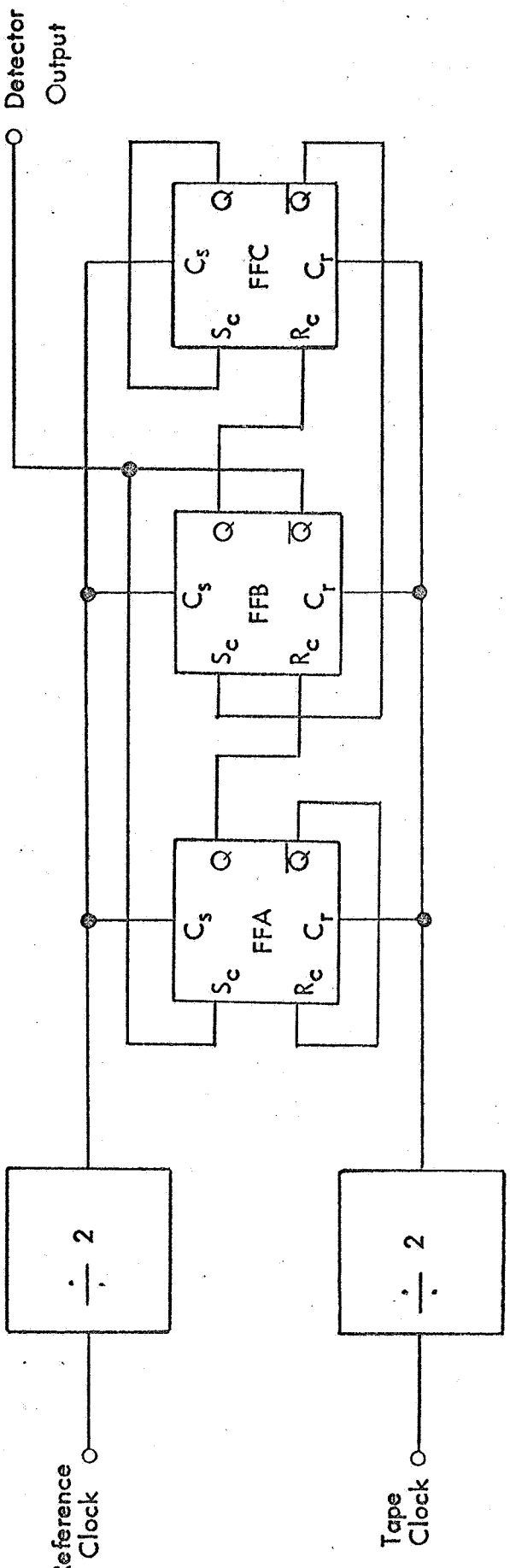

PHASE DETECTOR SCHEMATIC DIAGRAM

FIGURE 7

Reference Clock = S

Tape Clock = R

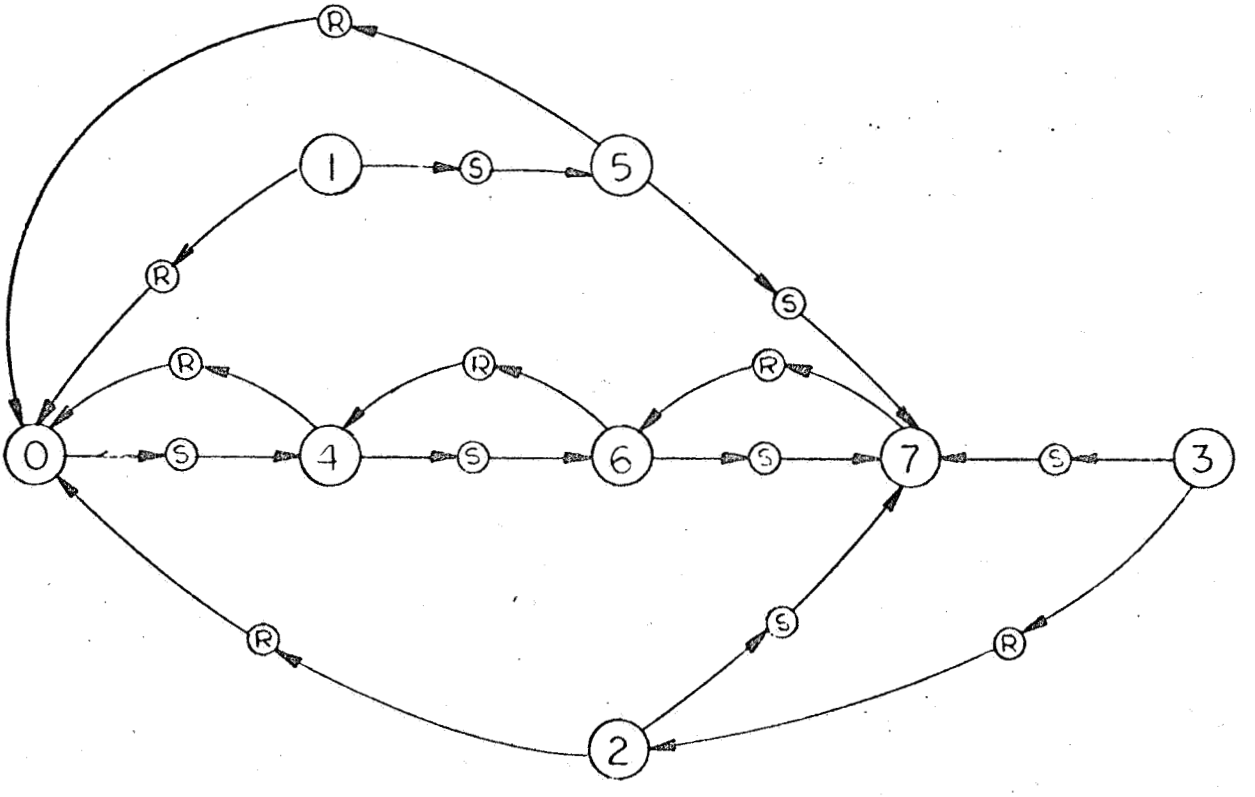

$FFA \Rightarrow 1$

$FFB \Rightarrow 2$

$FFC \Rightarrow 4$

i.e.: $FFA \cdot FFB \cdot FFC = 7$

$\overline{FFA} \cdot \overline{FFB} \cdot \overline{FFC} = 0$

PHASE DETECTOR STATE VARIABLE DIAGRAM

FIGURE 8

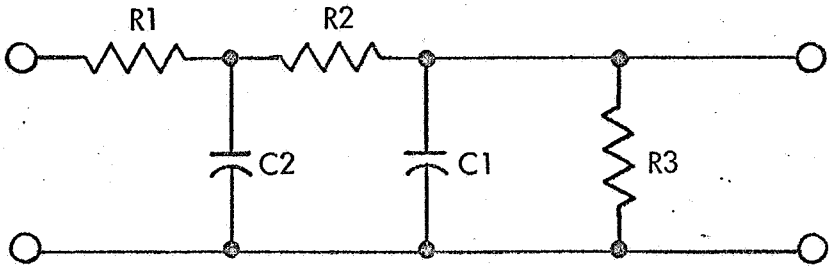

RC FILTER NETWORK

FIGURE 9

The remaining section of the servo amplifier shown in Figure 10 is essentially an operational amplifier within an operational amplifier. The interior operational amplifier is made up of the integrated circuit amplifier and the minor loop shown in Figure 11. The parameter values chosen conform to manufacturer's specification requirements to yield a closed loop gain of 1,000 volts/volt with a bandwidth of 1 megacycle. For consideration of the exterior minor loop, the closed loop gain of the interior operational amplifier may be considered as a forward gain element of 1,000 volts/volt, as shown in Figure 12. A nodal analysis of the circuitry of Figure 12 gives an open loop gain function

$$F_o(S) = \frac{5.2\,S\,(.00022\,S + 1)}{(.08\,S + 1)\,(.014\,S + 1)\,(.00025\,S + 1)}$$

The α portion of the Bode diagram for $F_o(S)$ is plotted in Figure 13. It may be observed that a slope of minus two exists only between 4k rad/sec and 4.5k rad/sec. Thus, a phase shift of 180° is never reached and the control amplifier minor loop is unconditionally stable.

The closed loop transfer function of the amplifier section may be found by considering node one (1) of Figure 10 to be a virtual ground. The closed loop transfer function is found to be

$$\frac{i}{e_1} = F_1(S) = \frac{.5\,(.071\,S + 1)\,(.01\,S + 1)}{(4.8\,S + 1)\,(.00022\,S + 1)} \quad \frac{\text{amps}}{\text{volt}}$$

The total servo amplifier transfer function is found by cascading the transfer functions of the three sections analyzed and is

$$F(S) = \frac{.08\,(.071\,S + 1)\,(.01\,S + 1)}{(4.8\,S + 1)\,(.001\,S + 1)\,(.00022\,S + 1)\,(.00016\,S + 1)} \text{ amps per radian}$$

2.5.2 Reference Clock Generator

The reference oscillator is a temperature compensated unijunction transistor, relaxation oscillator. The reference oscillator schematic is shown in Figure 14. Q1 and associated elements make up a voltage regulator to provide isolation from the primary supply. Q2, R1, and C1 form a conventional relaxation oscillator. Q3, R2, and R3 form a voltage regulator controlling the base 2 voltage of the UJT.

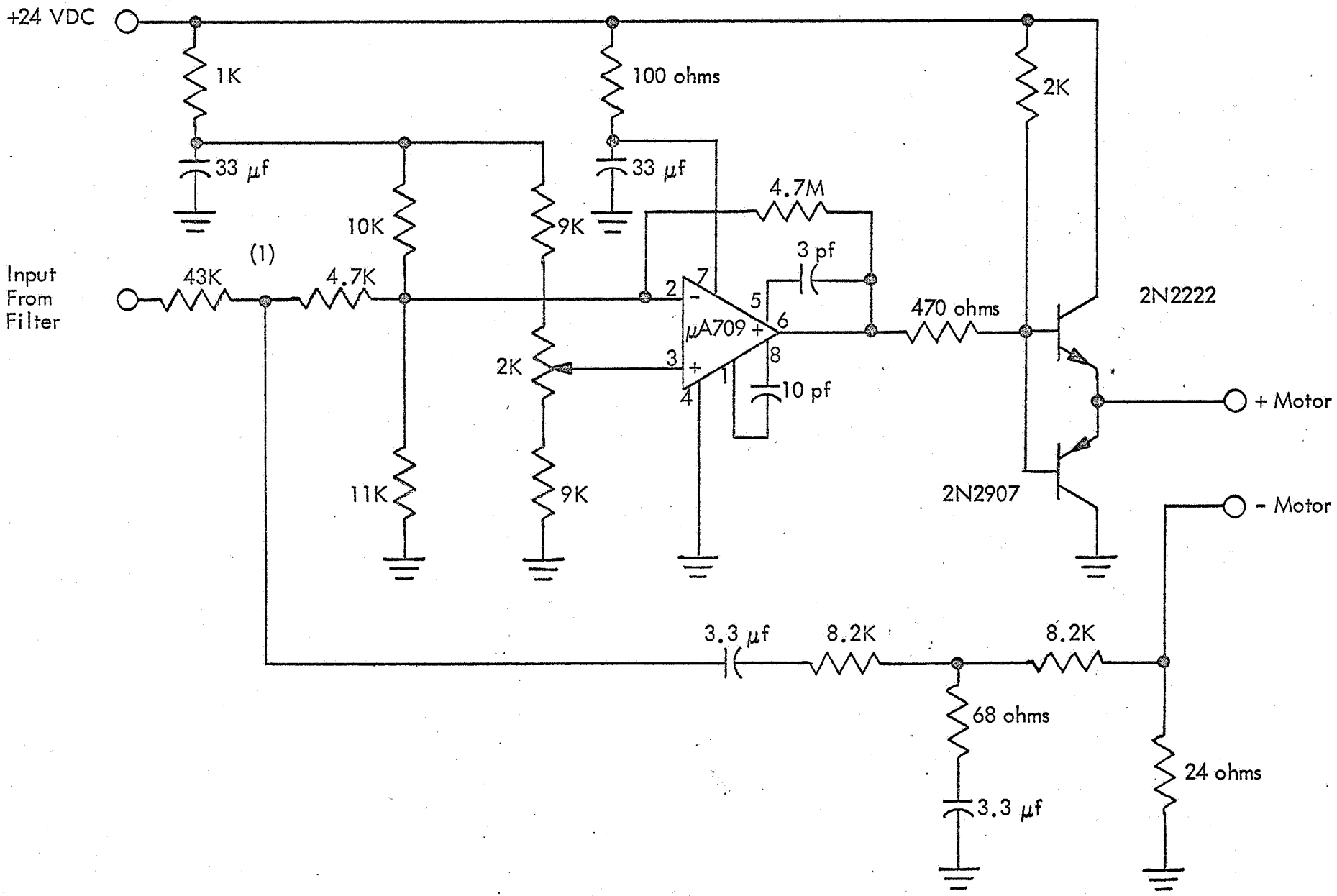

CONTROL AMPLIFIER SCHEMATIC

FIGURE 10

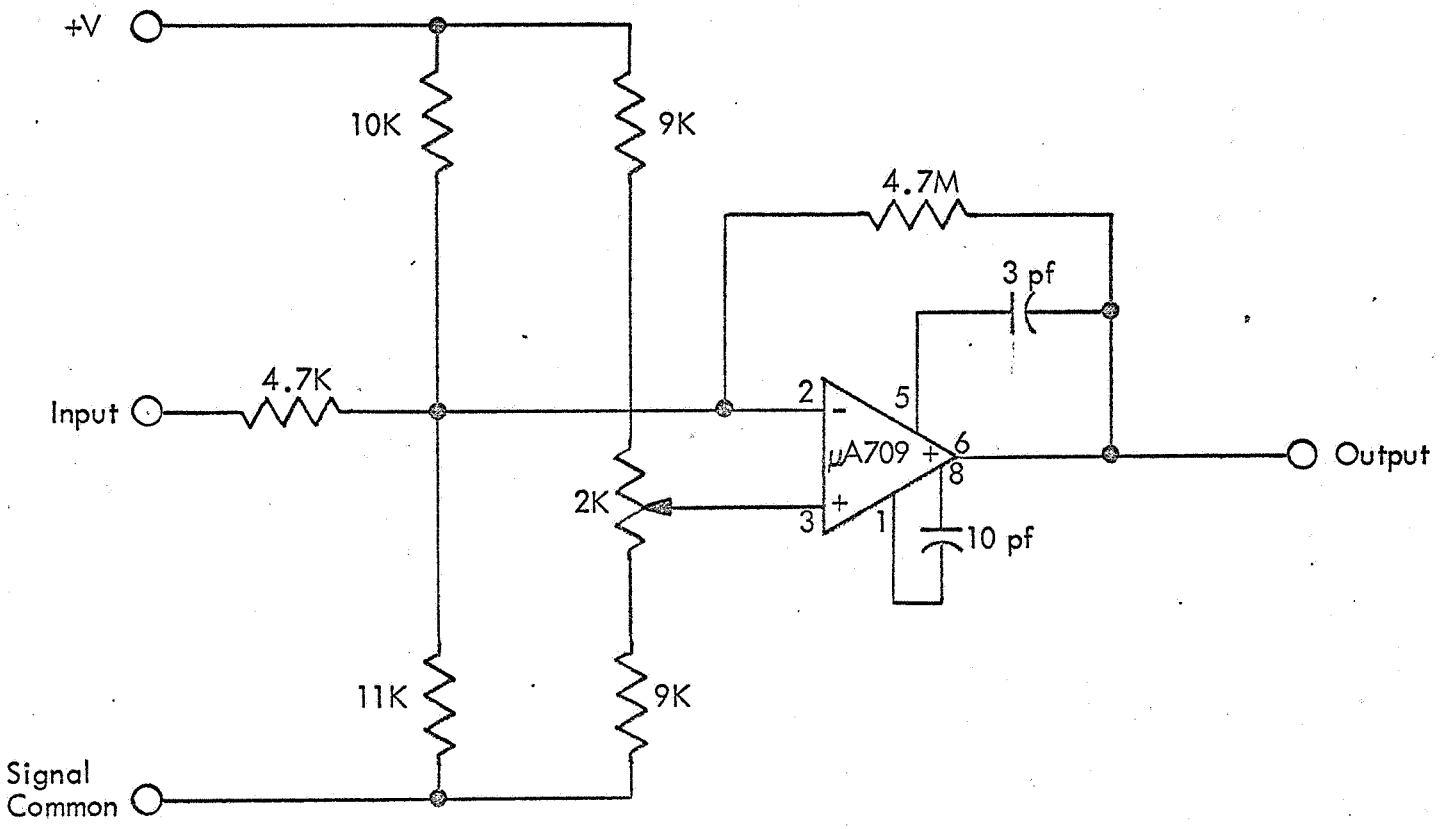

INTEGRATED CIRCUIT AMPLIFIER

FIGURE 11

$$F_o(S) = \frac{e_o}{e_1}, \quad A = 1000$$

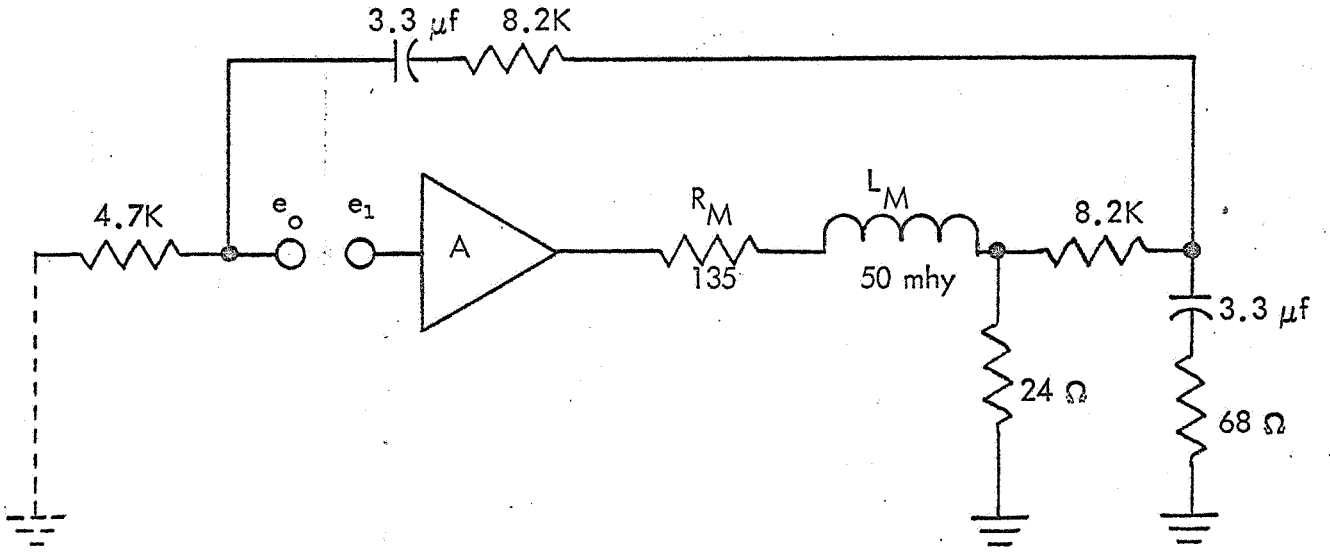

COMPENSATION CIRCUIT SCHEMATIC

FIGURE 12

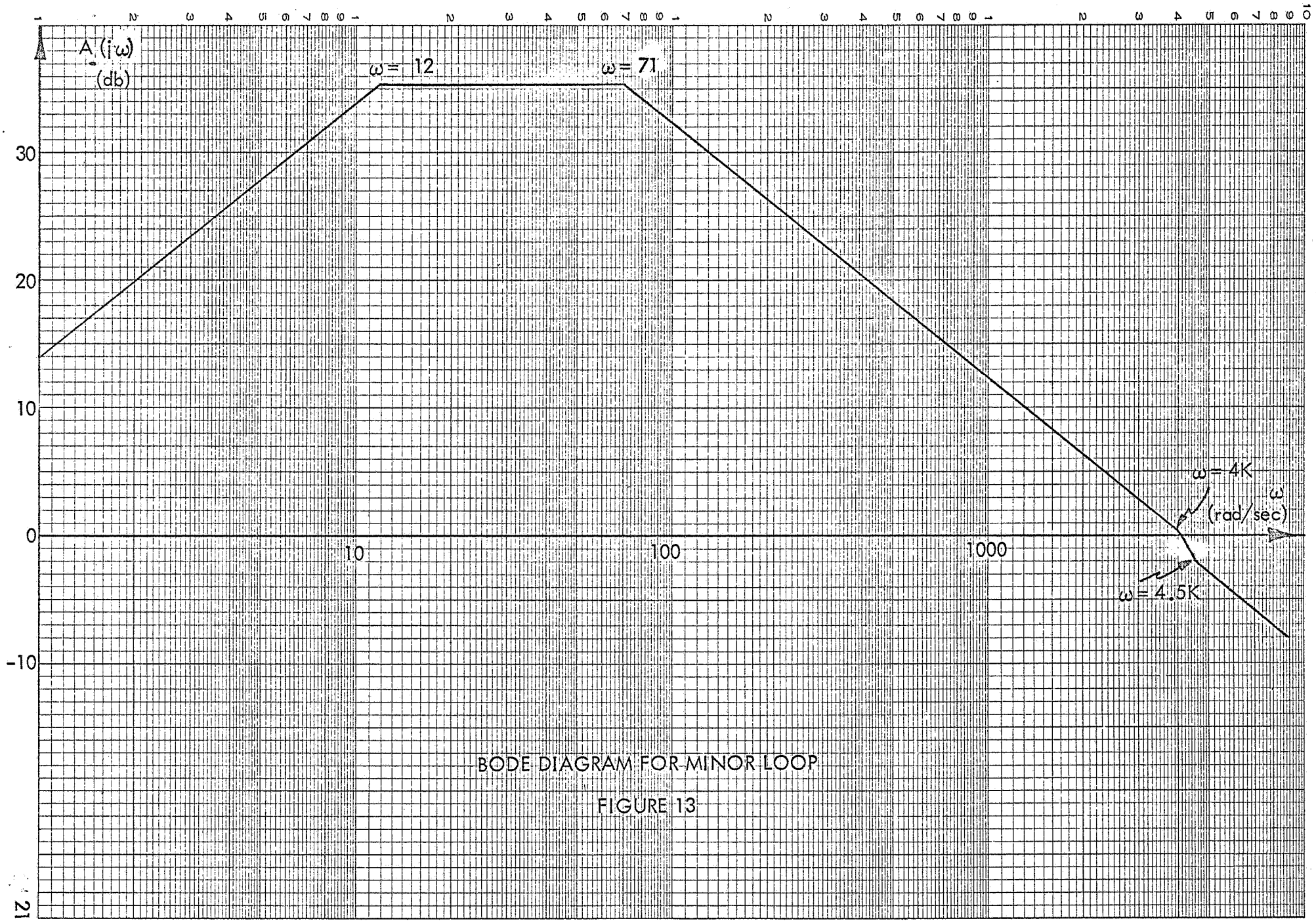

BODE DIAGRAM FOR MINOR LOOP

FIGURE 13

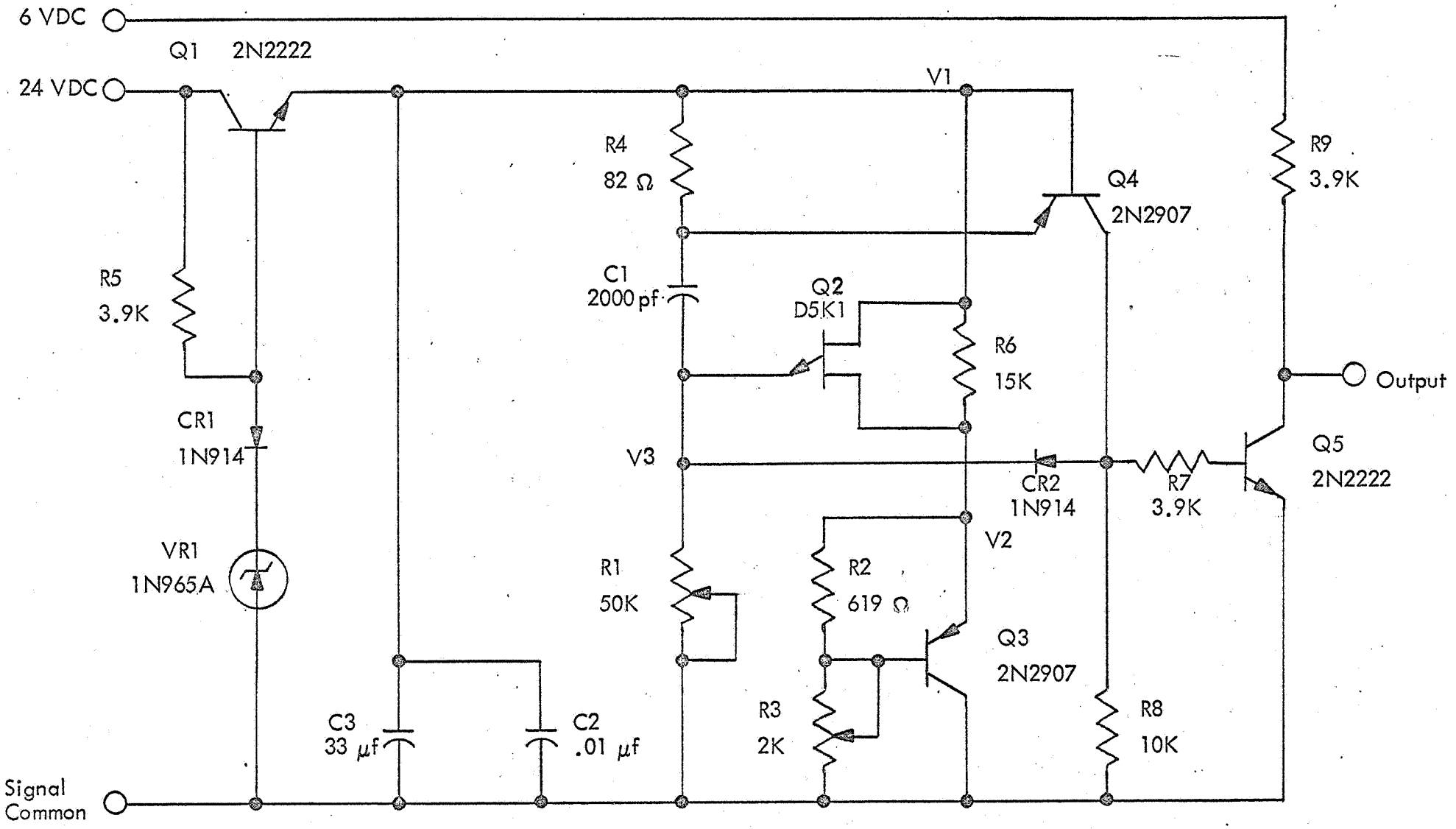

REFERENCE OSCILLATOR SCHEMATIC

FIGURE 14

The thermal characteristic of this regulator is adjusted by R3 to provide linear temperature compensation for the oscillator. Q4 and Q5 provide amplification for the pulse occurring at the regenerative transition of the oscillator. The amplified pulse is used to toggle a flip-flop, thereby providing a stable square wave. The accuracy of the oscillator is effectively limited only by the linearity of the temperature coefficients of Q2, Q3, R1, R2, R3, and C1. An analysis of the reference oscillator is given in the Appendix.

2.5.3 Data Electronics

The source of the servo feedback signal during the reproduce mode is the digital data stored on tape. NASA furnished equipment is used to amplify the signal off of the tape. The output of this equipment is a digital data signal reconstructed to the same signal as recorded on tape. The derivation and manipulation of the digital data necessary to provide a servo signal and to accommodate clocking of the reproduced data with a stable reference are discussed below.

2.5.3.1 BIØC To NRZC Converter and Clock Generator

The digital format used for data storage, as specified, is Bi-Phase Change (BIØC, also referred to as Manchester Code). Because of the inherent nature of this format to be self-clocking, i.e., at least one tape flux transition per data bit, it is not necessary to record a clock track on tape.

It is the function of the BIØC to NRZC Converter and Clock Generator to extract a clock signal from the BIØC data and to convert the BIØC data to NRZC data. The desired clock signal is a square wave, the frequency of which is equal to the data transfer rate, approximately 10k BPS. To insure the ability to clock the output data with a reference source, a dejittering buffer is used, as mentioned previously. To operate the buffer in a straightforward manner, it is desirable to convert the BIØC data to NRZC data. Figure 15 illustrates a BIØC input signal and the resultant clock and NRZC signals present at the output of the BIØC to NRZC Converter and Clock Generator.

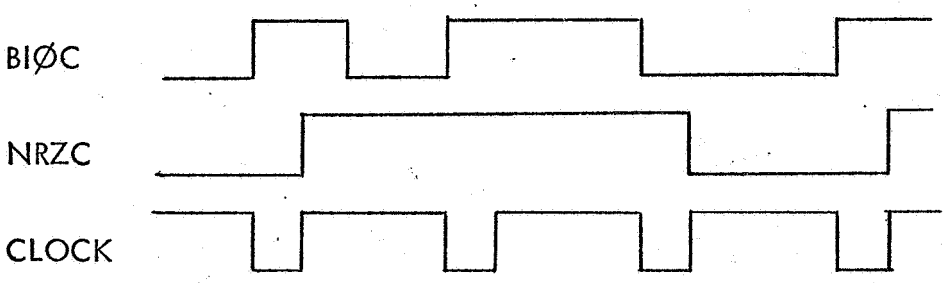

BIØC, NRZC, and CLOCK
Figure 15

To obtain the clock and the NRZC data (refer to Figure 16), the leading and trailing edges of the reproduced BIØC data are detected. The resultant pulses from the leading edge detector (LED) and trailing edge detector (TED) are used as gated trigger pulses to two identical monostable multivibrators. Each multivibrator output is used as the gating signal to the opposite multivibrator. This circuit configuration results in an effective inhibition of pulses derived from either the LED or TED which occurred at bit cell boundaries. Thus, the pulses which occur at bit cell centers, once per bit, are retained while all other pulses are removed. The resultant pulse train, occurring at the data rate, is used to trigger a third monostable multivibrator, the delay of which is set for one-quarter bit period. This multivibrator output provides a clock that will shift the level of the BIØC data at the three-quarter bit point into a flip-flop. Since the level of a BIØC bit at the three-quarter bit point is high for a logic value of "1" and low for a logic level of "0", sampling or shifting into a flip-flop at the 270° point of a bit results in the desired BIØC to NRZC conversion.

Successful data conversion and clock generation becomes impaired when bit-to-bit jitter at the data input exceeds 25% peak-to-peak. Error analysis and data results which appear elsewhere in this report verify that bit-to-bit, peak-to-peak jitter will not exceed 10%. A further requirement for unimpaired operation is that the digital data content must contain a logic value change from "1" to "0" or "0" to "1" at one point in the data. This is necessary to obtain the proper clock phase, i.e., the data must not be comprised of all "1's" or all "0's".

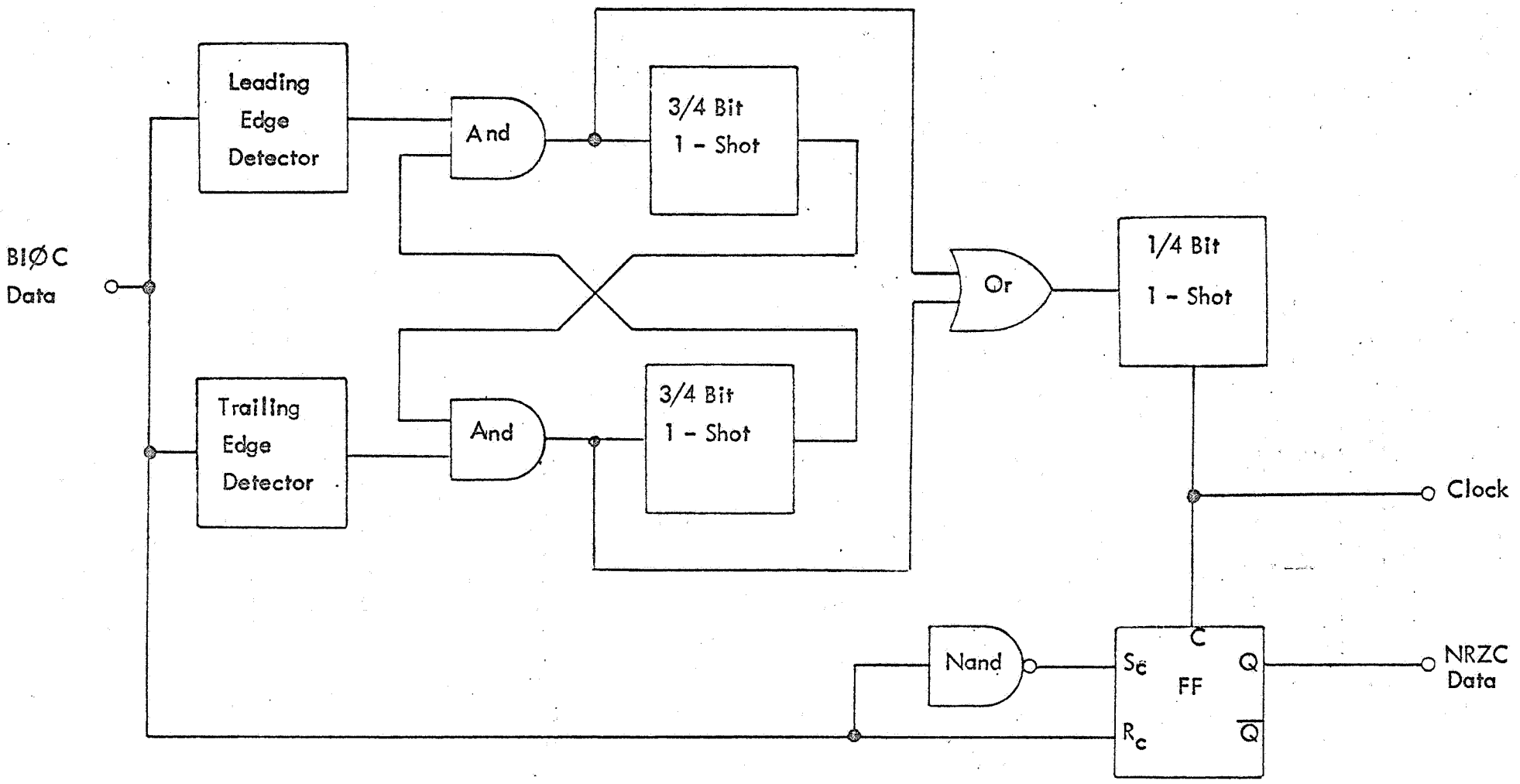

DATA CONVERTER AND CLOCK GENERATOR BLOCK DIAGRAM

FIGURE 16

2.5.3.2 Dejittering Buffer

As established earlier in this report, the anticipated maximum time base error is ±2 bits. This dictates the need for a 4-bit dejittering buffer to allow output clocking of data with the reference clock. To provide a safety margin of 100%, an 8-bit buffer is used. The buffer consists of eight storage flip-flops (see Figure 17), the outputs of which are bussed together through a gated OR. The data line is presented to the inputs of all eight flip-flops in parallel. The reconstructed tape clock signal is counted by a modulo 8 counter. As this counter is sequenced through its eight discrete states, a clock input signal is addressed sequentially from one storage flip-flop to another. Thus, at time decode load Ø (TDLØ) (see Figure 18), the status of the data line is transferred to FFØ (flip-flop Ø). At TDLI, the data is transferred to FFI, etc.

The reference clock is counted in a manner similar to the tape clock, with the resultant reference clock sequencer output used to sequentially address the data output gate on each flip-flop. Thus, at time decode unload Ø (TDUØ), the data stored in FFØ will be presented to the output buss. The state of the unload (reference clock) sequencer will nominally lag the load sequencer by 4 bits.

2.6 SERVO SYSTEM ANALYSIS

The primary control loop may be analyzed as a continuous system. Although the phase comparator is a binary device and should be treated as a sample and hold function, the equivalent sampling frequency is 5 kc, one-half the reference frequency which is sufficiently beyond the servo bandwidth to be ignored. In order to obtain a primary solution, the drive belt transmissibility is assumed to be unity. The primary control loop is shown in Figure 4 with appropriate transfer functions. The closed loop transfer function is found to be

$$\frac{C}{R} = \frac{(.071\,S + 1)\,(.01\,S + 1)}{(.0712\,S + 1)\,(.00692\,S + 1)\,(.000011\,S^2 + .0024\,S + 1)}$$

This transfer function is plotted in Figure 19.

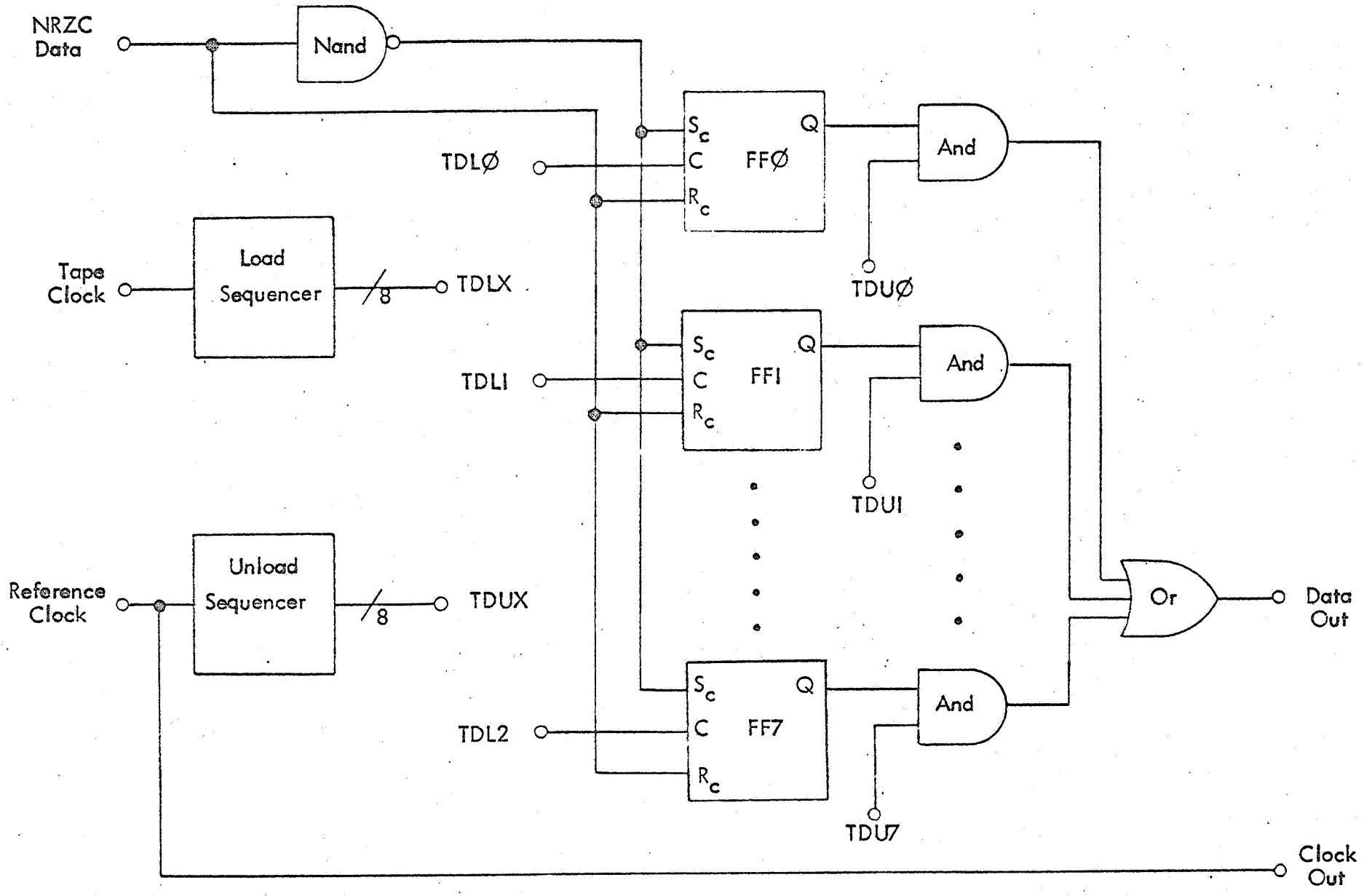

DEJITTERING BUFFER BLOCK DIAGRAM

FIGURE 17

BUFFER TIMING DIAGRAM, 8 BIT

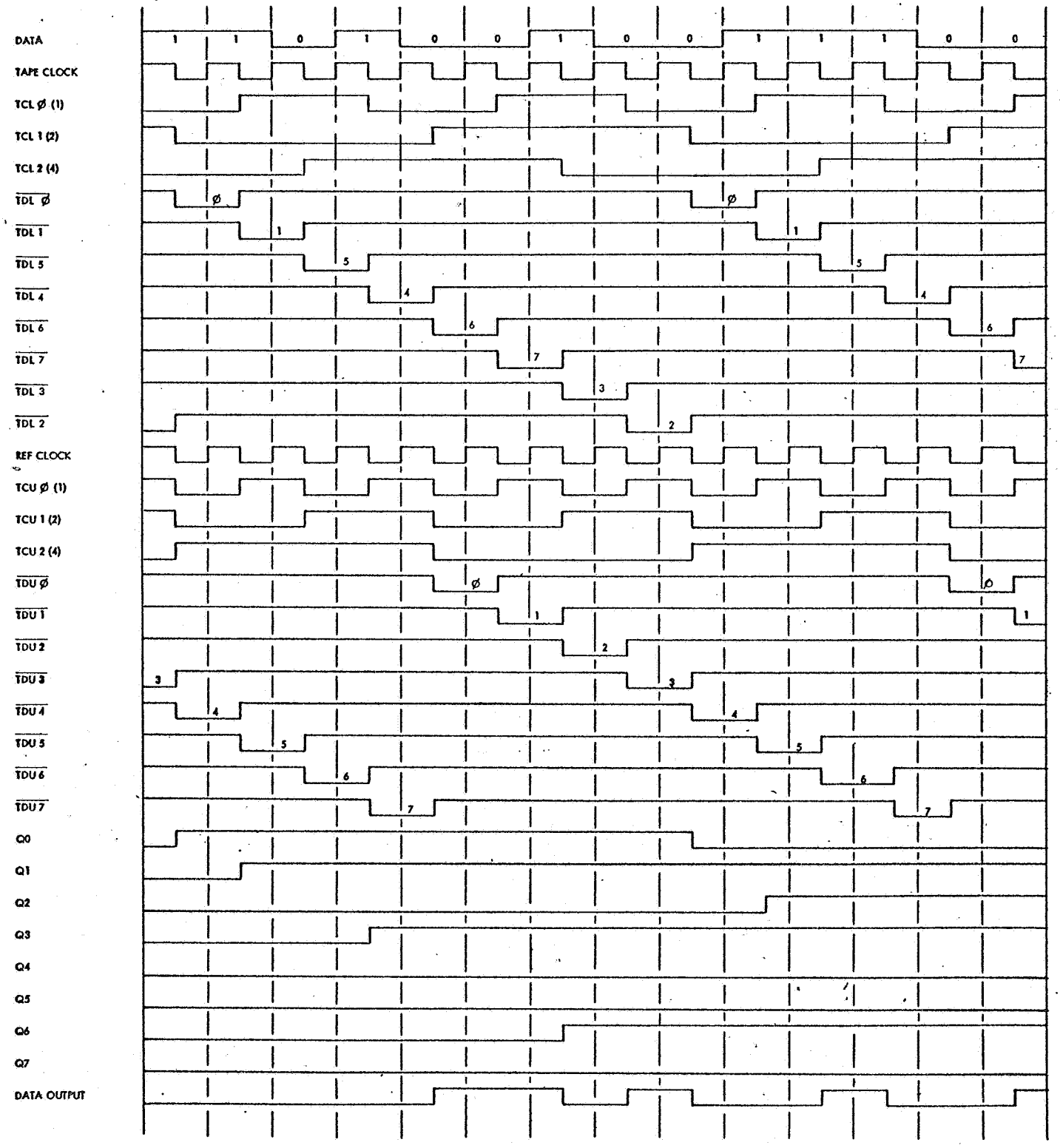

FIGURE 18

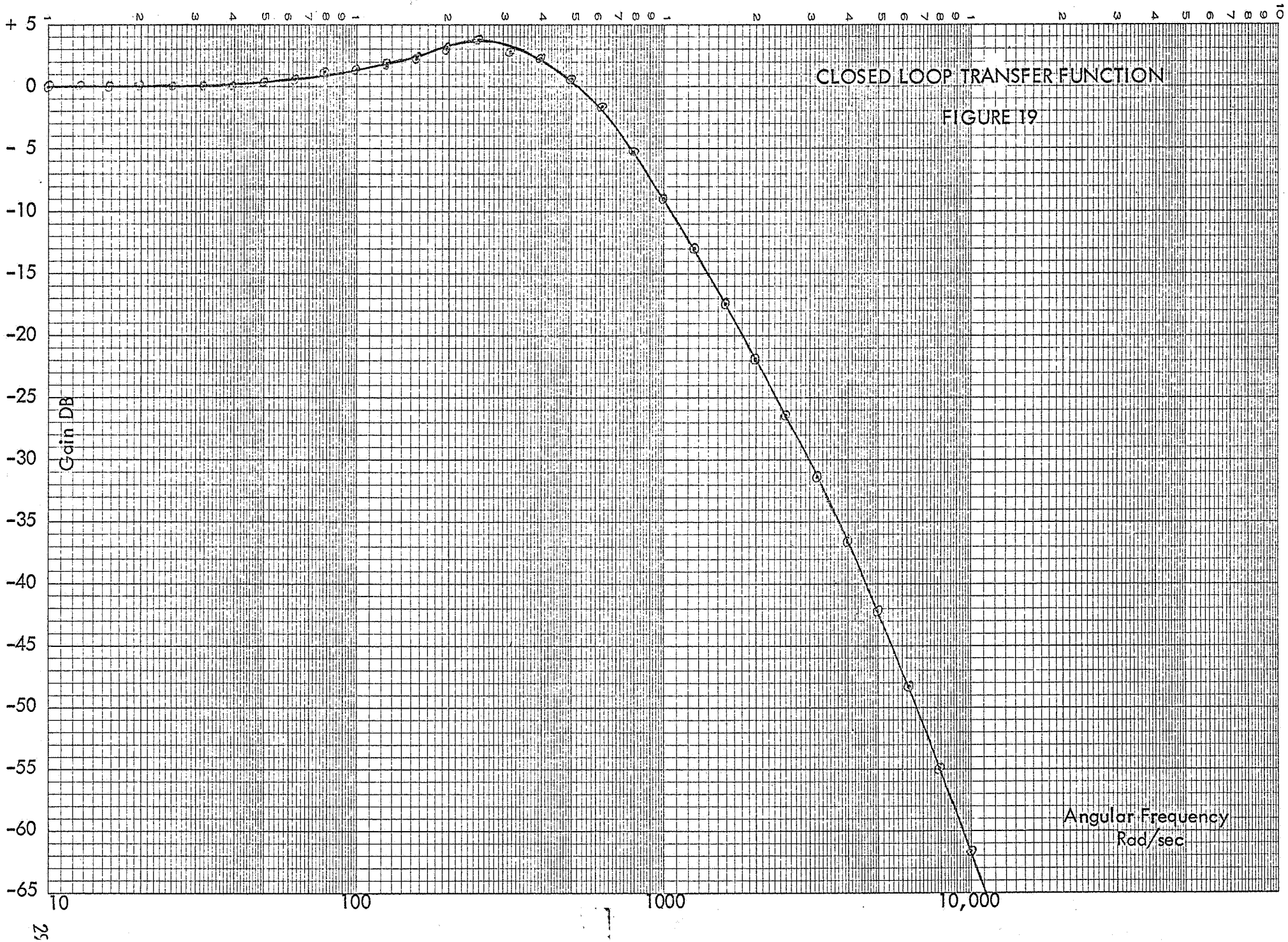

The expression $(1 - \frac{C}{R})$ is the tracking error coefficient and gives the ratio of closed loop flutter to open loop flutter for recorded flutter terms. The tracking error coefficient is plotted in Figure 20. This function is identical to the transfer function relating response in tape displacement to position error inputs $\frac{C_1(S)}{U_p(S)}$ as shown below:

$$1 - \frac{C}{R} = \frac{R - C}{R}$$

But: $R - C = \epsilon = \frac{R}{1 + GH}$

Where: GH = loop gain and H = unity

Thus: $1 - \frac{C}{R} = \frac{\epsilon}{R} = \frac{1}{1 + GH}$

Reference to Figure 4 shows that if $U_p(S)$ is considered the servo input, then $C_1(S)$ is the error term, ϵ, thus:

$$C_1(S) = \frac{U_p(S)}{1 + GH} \qquad \frac{C_1(S)}{U_p(S)} = \frac{1}{1 + GH} \qquad \text{Q.E.D.}$$

The stiffness of the servo is a term referring to the inverse of the steady-state response of the system to torque disturbances. All torque disturbances in the loop may be reflected to a common summing point and are designated as U_T in Figure 4. The response in tape displacement may be found from the transfer function $\frac{C_1(S)}{U_T(S)}$. From the loop gain terms of Figure 4, the transfer function is found to be:

$$\frac{C_1(S)}{U_T(S)} = \frac{116\,(4.8\,S + 1)\,(.001\,S + 1)}{(.0712\,S + 1)\,(.00692\,S + 1)\,(.000011\,S^2 + .0024\,S + 1)}$$

The inverse of stiffness, $\frac{C_1(S)}{U_T(S)}$, is plotted in Figure 21.

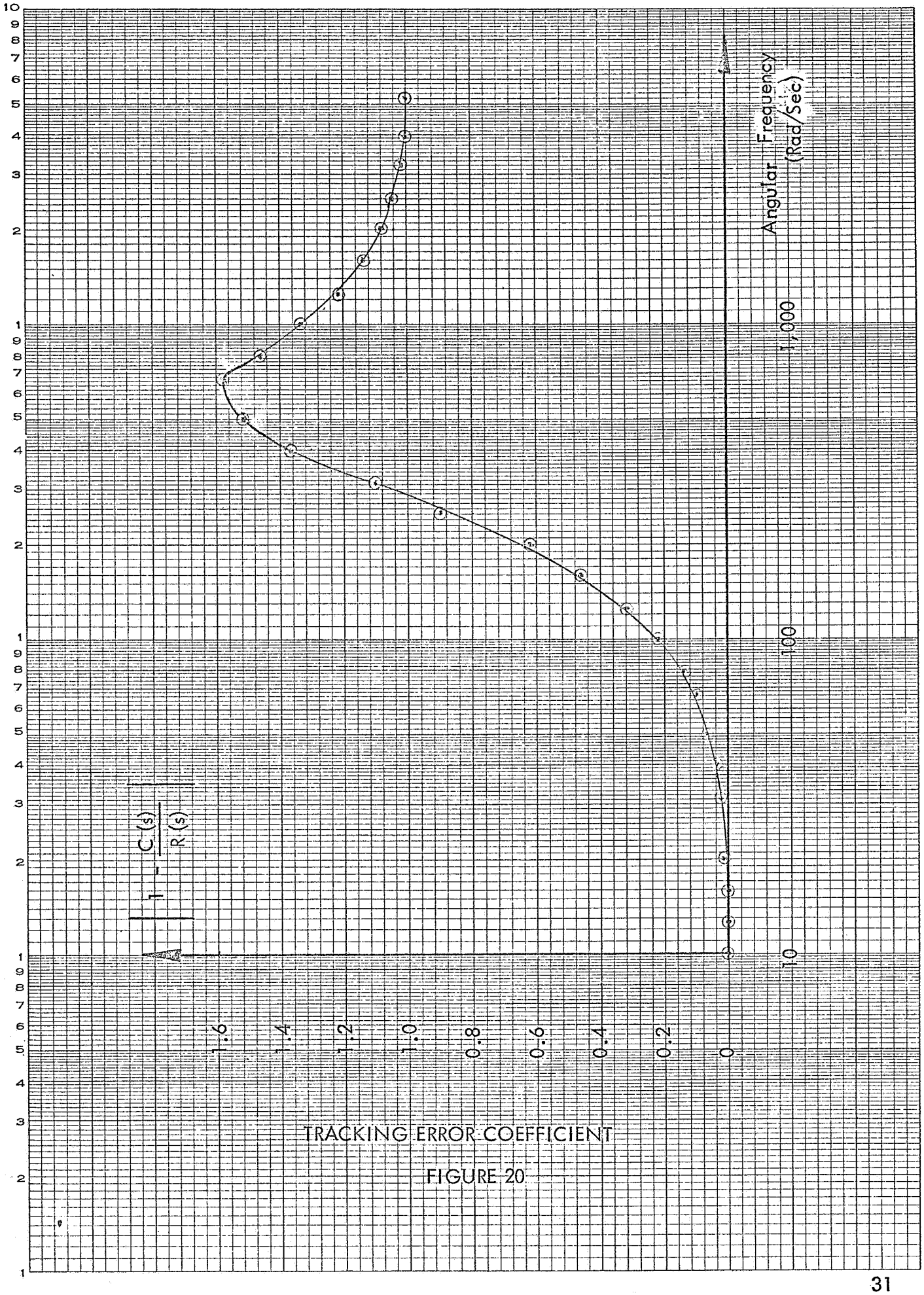

TRACKING ERROR COEFFICIENT

FIGURE 20

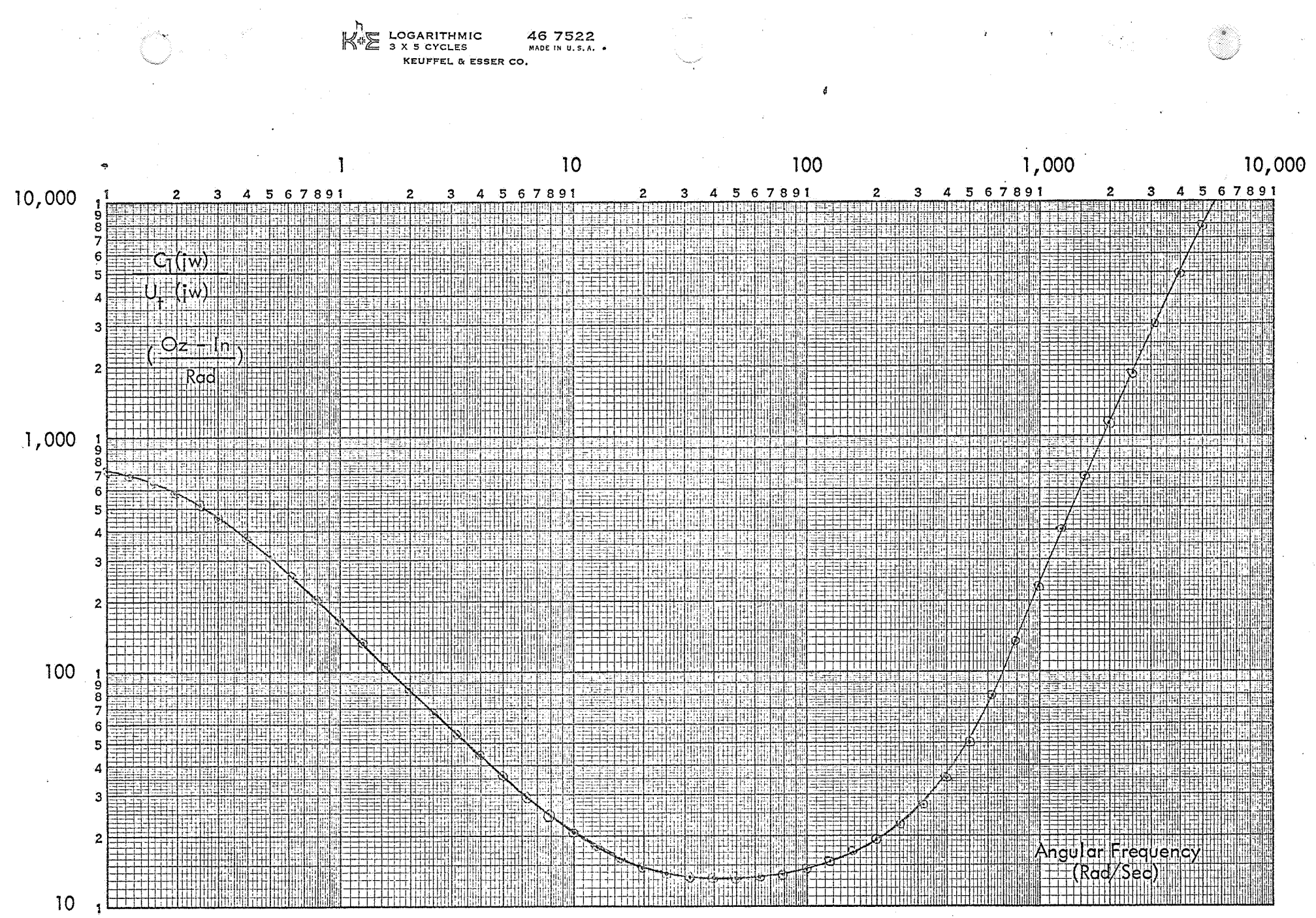

INVERSE STIFFNESS PLOT

FIGURE 21

The unit step response of the system is found from the closed loop transfer function for $R(S) = \frac{1}{S}$.

$$C(S) = \frac{(.01\,S + 1)}{S\,(.0069\,S + 1)\,(.000011\,S^2 + .0024\,S + 1)}$$

The inverse Laplace Transformation yields

$$C(t) = \mu(t) + .5\,e^{-144t} - 1.56\,e^{-109t}\,\mathrm{Sin}\,(280\,t + 1.3)$$

C (t) is plotted in Figure 22.

The secondary control loop may be analyzed in terms of the primary control step response. The secondary control effects an equivalent one bit position step command to the primary control loop when the buffer status detector detects a buffer load-unload relationship more than one bit from nominal. However, a one bit step will saturate the phase detector in the control amplifier. The step response of Figure 22 reveals that a one bit displacement requires approximately 10 milliseconds. This tims is equivalent to 125 sample times of the sync status indicator; therefore, the phase comparator will be held in saturation.

During this time an over-correction equal to the difference between the linear and mnemonic range of the phase comparator will occur. The over-correction is one bit. Since the secondary control loop has a built-in one bit dead zone the one bit over-correction will return the buffer to nominal status. The time required to effect this compensation is approximately

$$t_c = n\,t_r$$

Where

n = displacement error in bits

t_r = servo rise time

$t_r \approx 10$ milliseconds

2.7 SERVO SYSTEM PERFORMANCE

The intrinsic error mechanisms of the transport assume two basic forms when related to the servo loop. These are position disturbances and torque disturbances. Position

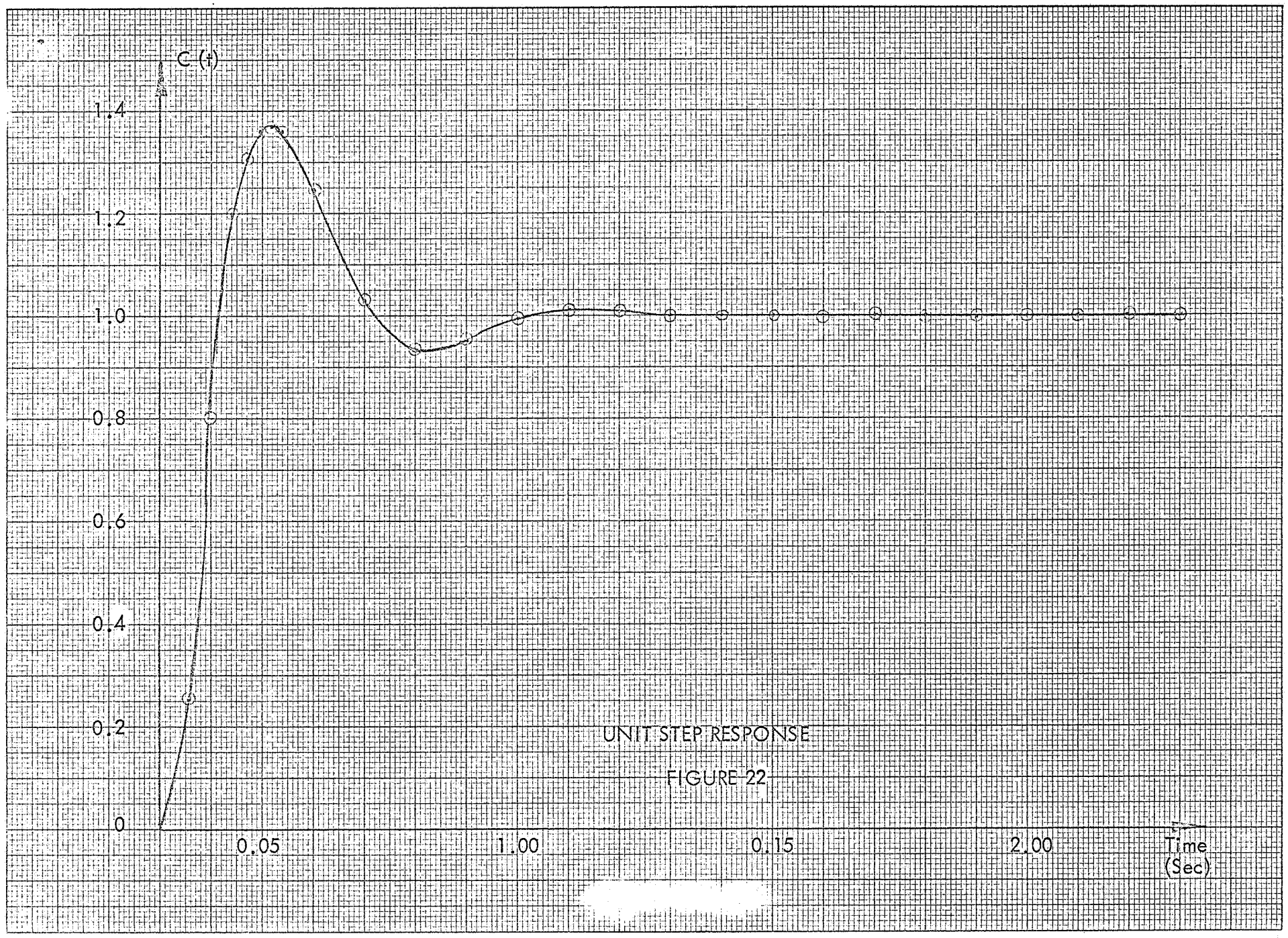

UNIT STEP RESPONSE

FIGURE 22

disturbances or position command errors include recorded jitter, whatever the source, and transfer ratio errors during playback such as those due to eccentricity. Torque disturbances include motor ripple torque, static and dynamic friction, dynamic unbalance, and reel load variations.

Ideal servo behavior exists when the servo tracks all position command errors perfectly and is insensitive to all torque disturbances. The two error forms may be reflected to the summing points shown in Figure 4. The servo performance is then measured by the transfer functions

$$\frac{C_1(S)}{U_p(S)} \text{ and } \frac{C_1(S)}{U_t(S)} .$$

These functions are plotted in Figures 20 and 21, respectively. The steady-state tape displacement error for a given error spectrum is given by

$$E(S) = \sum_{i=1}^{n} \frac{C_1(S)}{U_p(S)} \times U_p(S_i) \Bigg|_{S=S_i} + \sum_{k=1}^{m} \frac{C_1(S)}{U_t(S)} \times U_t(S_k) \Bigg|_{S=S_k}$$

The only predictable torque disturbance is the motor ripple torque given in Section 2.2. The resultant error term is:

$$E_{t1} \text{ ripple torque error} = \frac{\text{percent ripple} \times \text{running torque}}{\text{inertia (ripple frequency)}^2} \times \text{transport characteristic}$$

$$E_{t1} = \frac{(.2)\,(.07)\,(.085)}{(.55)\,(37)} = 5.7 \times 10^{-5} \text{ inches}$$

The ripple error term is a fraction of the data bit wave length, equal to 3.3×10^{-4} inches.

Figure 23 shows the flutter spectrum of the tape signal without servo control.

Figure 24 shows the effects of the flutter interpreted in terms of peak time base error.

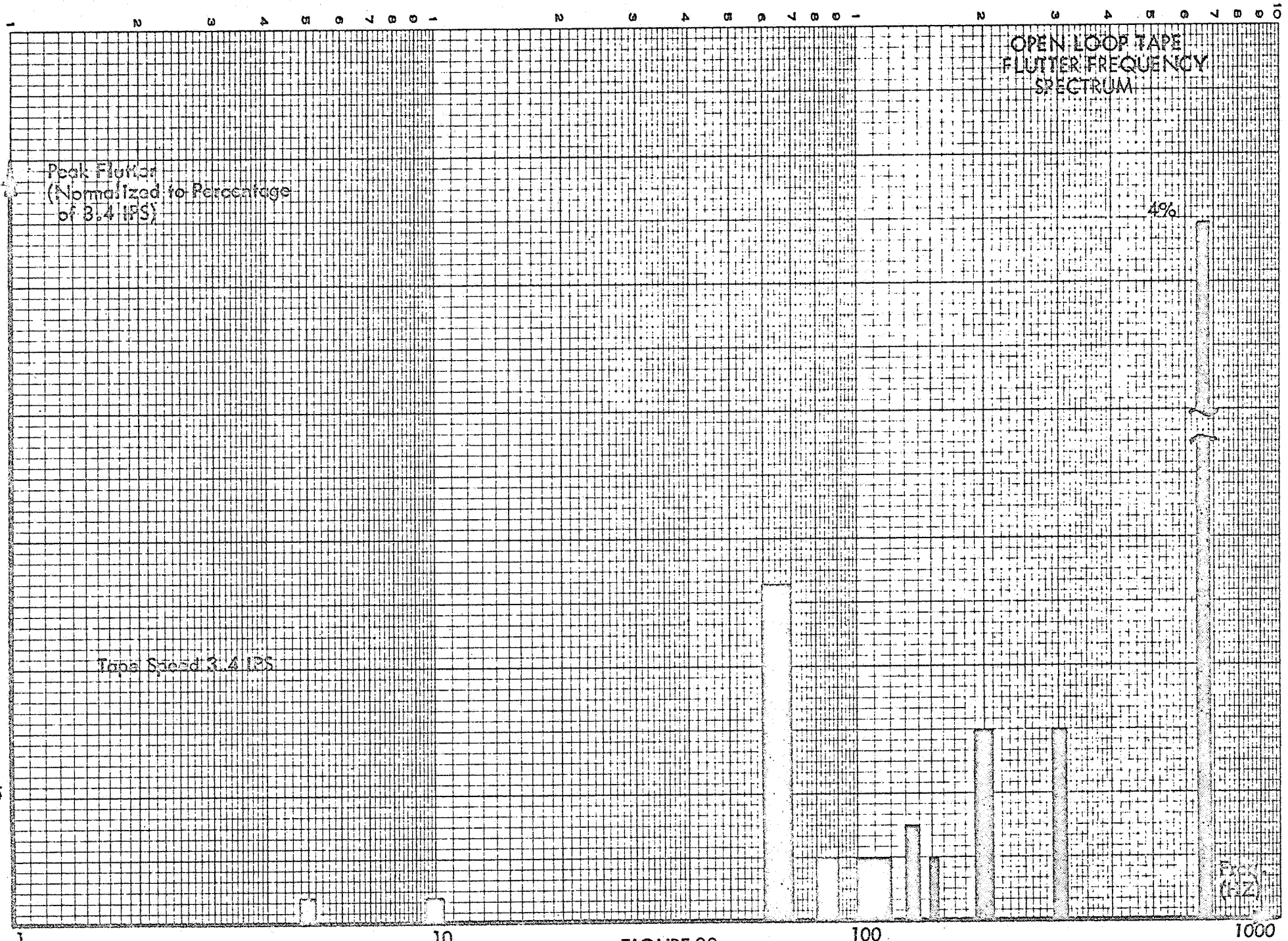

FIGURE 23

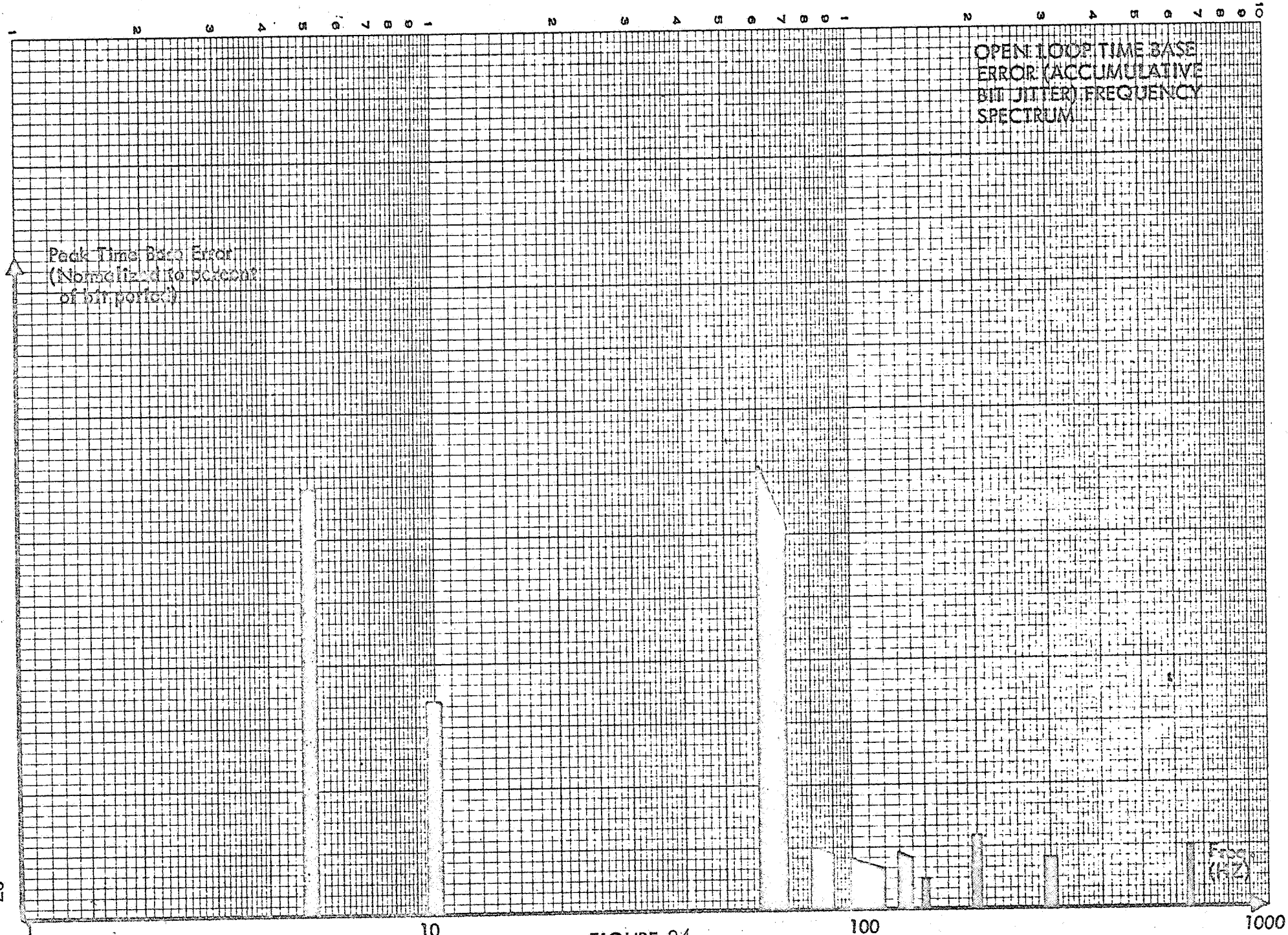

FIGURE 24

Figure 25 shows the spectrum of uncompensated time base error under servo control as previously discussed. It may be noted that the aggregate of uncompensated displacement error exceeds one-half of a bit width. Two bits of dejittering buffer storage are therefore required to accommodate peak-to-peak, steady-state servo error.

In addition, random transients are observed and require an additional two bits of storage.

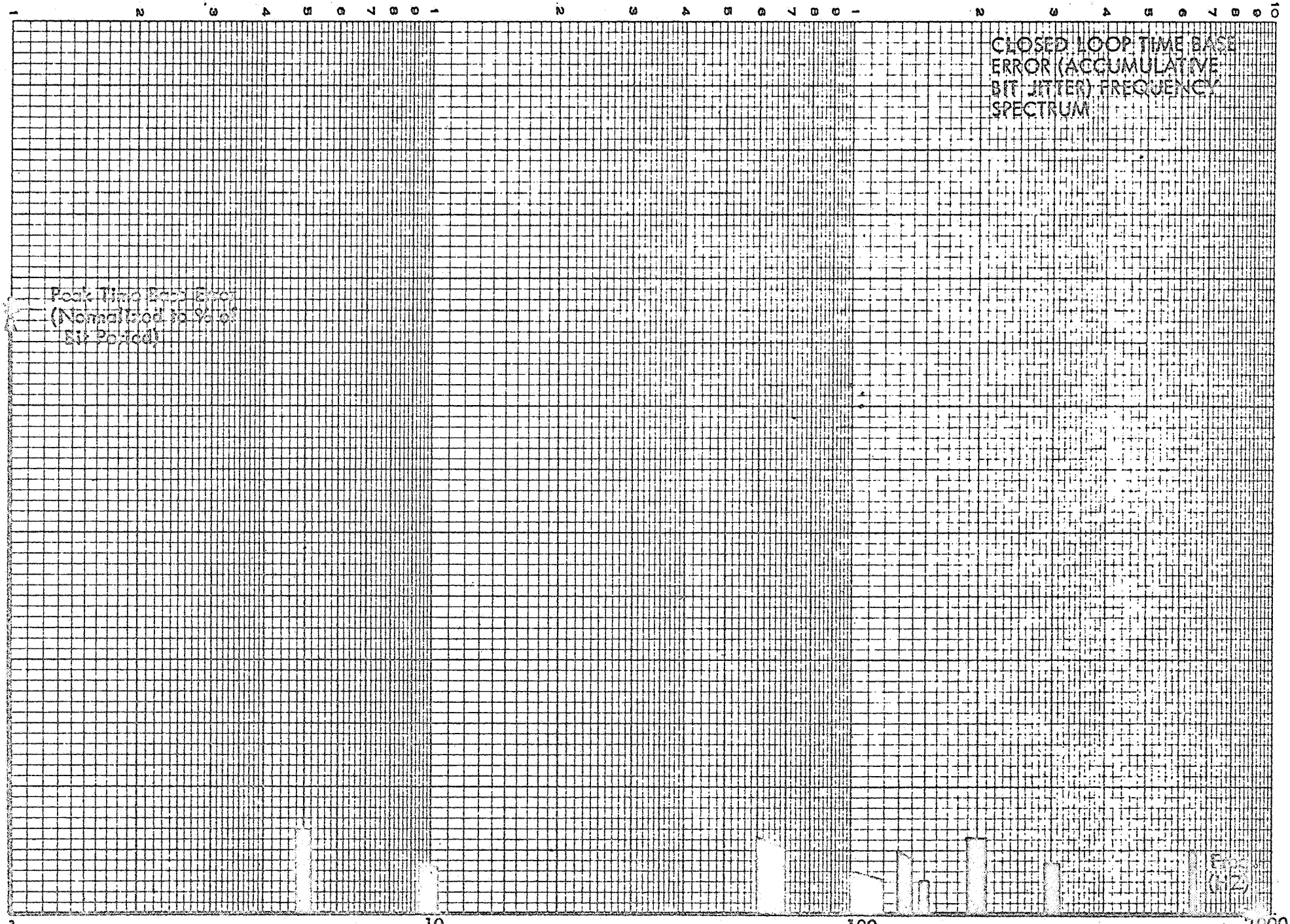

FIGURE 25

3.0 CONCLUSIONS

It is felt that the prototype system satisfies the requirements of the contracted study and development project. The effort conducted in this program has yielded a significant step forward in the tape recorder technology for space applications, namely, a basic phase-locked servo and dejittering buffer electronics package that can be produced and used as a basic building block in many space applications. The packaged system is shown in Figure 26.

The total electronics package encompasses a volume of 32.5 cubic inches, weighs 15 ounces, and requires 1.5 watts average power, 4 watts transient power. The study was conducted by operating the recorder at 0.133 ips record speed while recording a 400 bits/second data rate, resulting in a 3,000 bits per inch packing density. The playback performance was evaluated at 3.3 ips and a playback data rate of 10k bits per second. A record-to-playback ratio of 25:1 was the basis of the study requirement.

The test and evaluations conducted on the NASA Goddard furnished transport showed that a servo correction bandwidth of 70 Hz was achieved. Errors produced above 70 Hz are removed by an 8-bit buffer. The evaluation showed that a 4-bit buffer was sufficient; however, an 8-bit buffer was utilized to provide a safety margin.

System design emphasis was placed upon minimizing the changes required to accommodate different data rates. This was accomplished by locating all rate sensitive components on the mother boards.

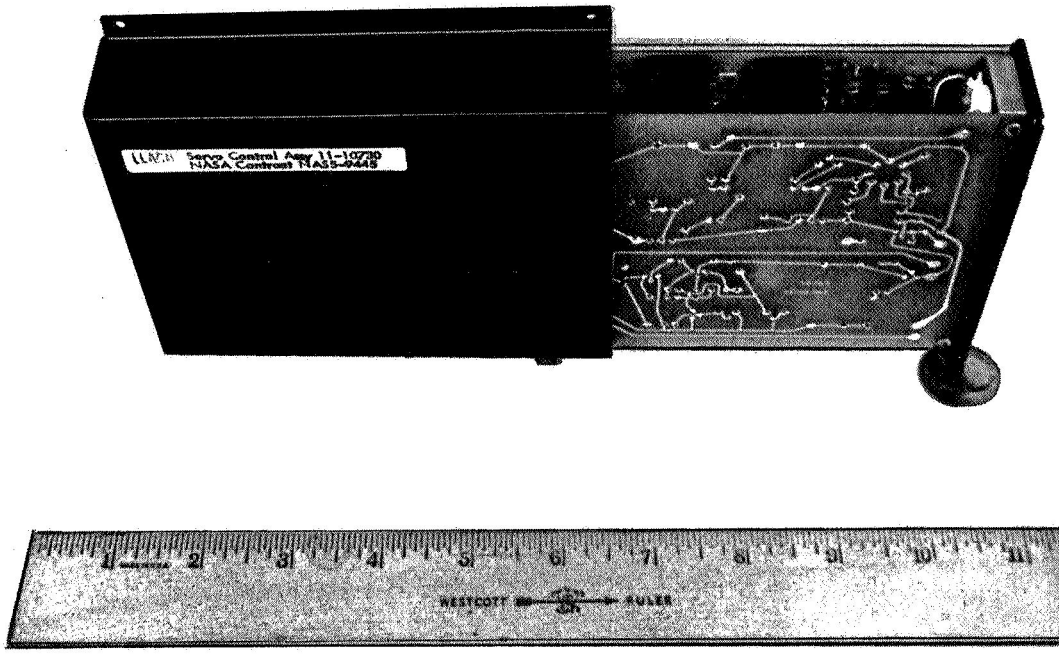

00507

SYSTEM ASSEMBLY

FIGURE 26

APPENDIX I

ECCENTRICITY ANALYSIS

Eccentricity of drive shafts is a source of tape jitter and may be analyzed as follows. Consider a shaft with a true center and center of rotation as shown in Figure A1-1.

C_t = true center

r = true radius

C_s = center of rotation

e = eccentricity (absolute)

ω = shaft angular velocity

v_i = instantaneous tangential velocity

r_i = instantaneous radius of rotation

$v_i = r_i \omega$

By the law of Cosines

$$r^2 = e^2 + r_i^2 - 2 e r_i \operatorname{Cos} \theta$$

$$\theta = \omega t$$

Solving equation (1) for r_i yields:

$$r_i = e \operatorname{Cos} \theta + e^2 \operatorname{Cos}^2 \theta + r^2 - e^2$$

Since $r >> e$

$$r_i = r + e \operatorname{Cos} \theta$$

Or

$$r_i \approx r \left(1 + \frac{e}{r} \operatorname{Cos} \omega t\right) \qquad (2)$$

And

$$v_i \approx \omega r \left(1 + \frac{e}{r} \operatorname{Cos} \omega t\right) \qquad (3)$$

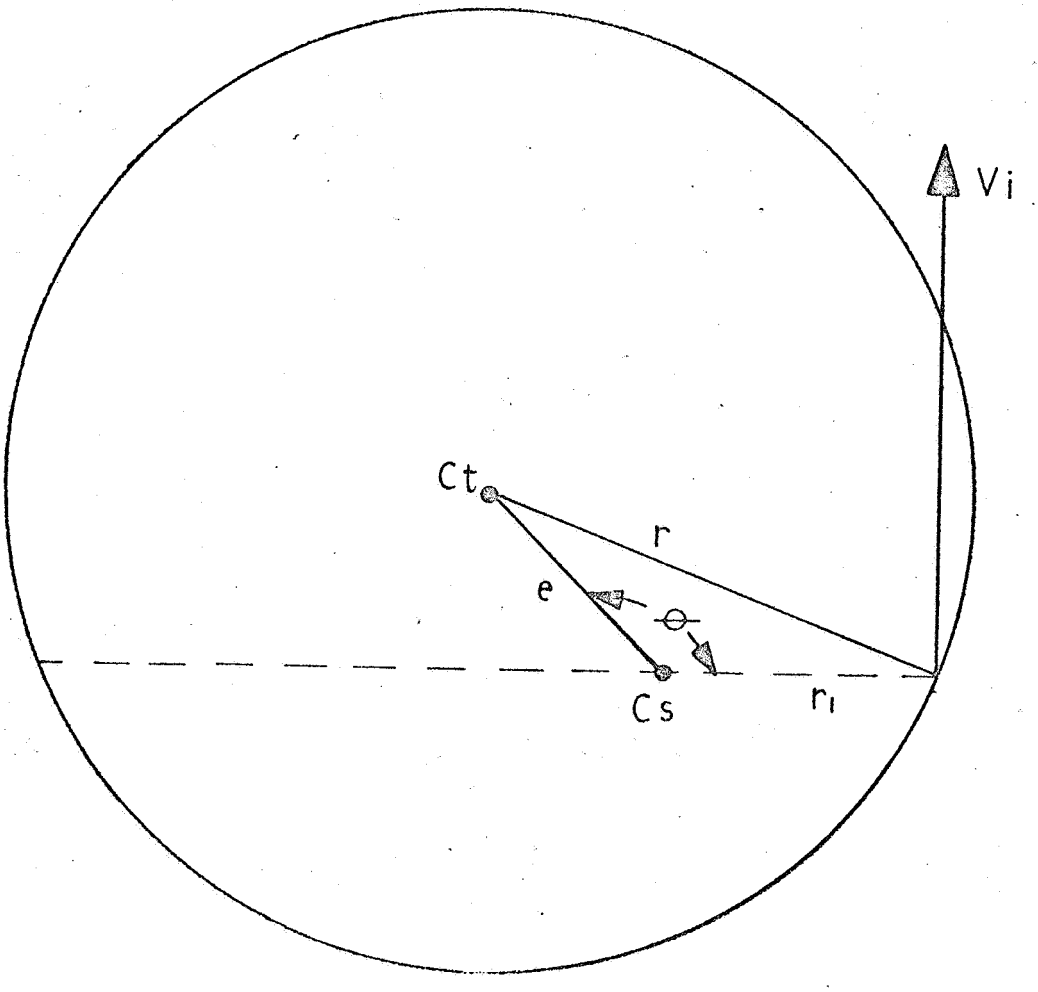

DIAGRAM OF ECCENTRICITY

FIGURE A I-1

In a belt drive system the transmission ratio is equal to the ratio of shaft radii at the points of contact. Transmitted speed will therefore assume the form of equation (2). That is, transmitted speed will be modulated at a once per revolution rate at a percentage proportional to percentage eccentricity. One, therefore, expects the smallest shafts to exhibit the largest flutter due to eccentricity, assuming the same shaft speeds. Table I gives the eccentricities measured and the resultant predicted flutter terms.

Flutter frequency multiplication due to non-unity record to playback speed ratios is a well known tape phenomena. References* show that for a record tape speed of the form

$$v_r = V_{or} (1 + a \cos \omega_1 t)$$

And a playback tape speed of

$$v_{pb} = v_{opb} (1 + b \cos \omega_2 t)$$

The aggregate flutter of the tape signal for playback will have the form

$$e_f = K\, b \cos \omega_2 t - a \cos \frac{v_{obp}}{v_{or}} \omega_1 t + b \frac{v_{opb}\, \omega_1}{v_{or}\, \omega_2} \sin \omega_2 t \qquad (4)$$

Equation (4) shows that a record flutter component is scaled in frequency by the speed ratio and frequency modulated by the playback flutter scaled in proportion to the speed ratio and inversely proportional to the flutter frequency ratio. For flutter terms proportional to tape speed, as is the case for eccentricity, equation (4) reduces to

$$e_f = K\, b \cos \omega_2 t - a \cos \frac{v_{opb}}{v_{or}} \omega_1 t + b \sin \omega_2 t$$

*Davies, Magnetic Tape Instrumentation, McGraw-Hill, 1961.

APPENDIX II

TRANSMISSIBILITY ANALYSIS

The design of high performance servos typically requires consideration of mechanical parasitics. Consider a simple belt drive system of Figure AII-1, where

T_1 = input torque

T_2 = output torque

J_1 = inertia of assembly 1

J_2 = inertia of assembly 2

r_1 = radius of assembly 1

r_2 = radius of assembly 2

K = belt spring constant

D = viscous damping coefficient

The characteristic equations for the shaft assemblies are:

$$T_1 = J_1 \ddot{\theta}_1 + D_1 \dot{\theta}_1 2 r_1 \ (r_1 \theta_1 - r_2 \theta_2) K$$

$$0 = J_2 \ddot{\theta}_2 + D_2 \dot{\theta}_2 2 r_2 \ (r_1 \theta_1 - r_2 \theta_2) K + T_2$$

In Laplace form:

$$T_1(S) = (J_1 S^2 + D_1 S + 2r_1{}^2 K) \ \theta_1(S) - 2K r_1 r_2 \theta_2 (S)$$

$$0 = (J_2 S^2 + D_2 S + 2r_2{}^2 K) \ \theta_2(S) - 2K r_1 r_2 \theta_1(S) + T_2(S)$$

If the output torque is constant and interest is restricted to dynamic behavior, $T_2(S)$ may be set to zero. Simultaneous solution of the above equation yields:

$$\frac{\theta_1 (S)}{T_1 (S)} = \frac{J_2 S^2 + D_2 S + 2r_2{}^2 K}{(J_1 S^2 + D_1 S + 2r_1{}^2 K) \ (J_2 S^2 + D_2 S + 2r_2{}^2 K) - (2r_1 r_2 K)^2}$$

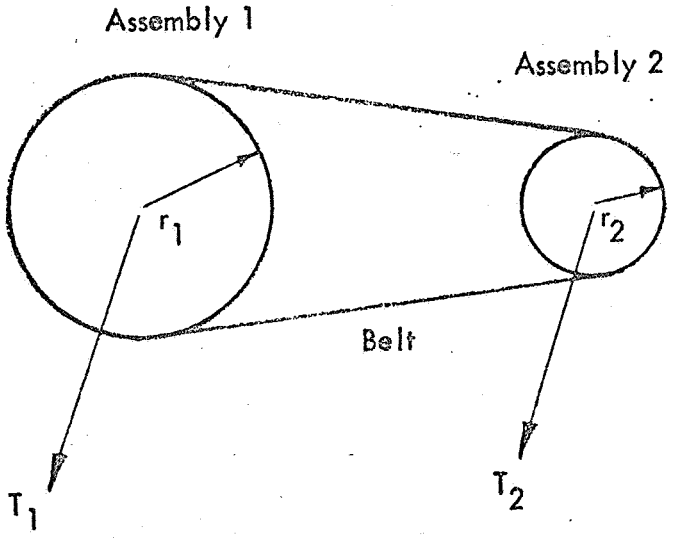

SIMPLE BELT DRIVE SYSTEM

FIGURE A II-1

Also

$$\frac{\theta_2(S)}{\theta_1(S)} = \frac{2r_1 r_2 K}{(J_2 S^2 + D_2 S + 2Kr_2^2)}$$

The transfer function, $\frac{\theta_2(S)}{\theta_1(S)}$, is defined as the transmissibility of the system.

Neglecting viscous damping terms D_1 and D_2, the characteristic equation

$$(J_1 S^2 + D_1 S + 2r_1^2 K)\ (J_2 S^2 + D_2 S + 2r_2^2 K) - (2r_1 r_2 K)^2 = 0$$

Reduces to

$$J_1 J_2 S^4 + (r_2^2 J_1 + r_1^2 J_2)\ 2KS^2 = 0$$

Or

$$J_1 J_2 S^2 (S^2 + \omega_n^2) = 0$$

Where

$$\omega_n = \left[2K\left(\frac{r_2^2}{J_2} + \frac{r_1^2}{J_1}\right)\right]^{1/2}$$

ω_n is the natural frequency of the system. It may be assumed that noise and transients will always be present to excite this resonance and produce an error term at the natural frequency with a magnitude depending on the viscous damping in the system. In addition, servo stability will be affected for servo bandwidths near ω_n because of the additional poles to be considered.

From the preceding derivations we may write:

$$\frac{\theta_1(S)}{T_1(S)} = \frac{1}{J_1 S^2} \quad \frac{(S^2 + 2\zeta_2 \omega_{n2} S + \omega_{n2}^2)}{(S^2 + 2S_{12} \omega_{n12})}$$

$$\frac{\theta_2(S)}{\theta_1(S)} = \frac{r_1 r_2 K}{J_2} \quad \frac{1}{(S^2 + 2\zeta\,\omega_{n2}\,S + \omega_{n2}{}^2)}$$

And

$$\frac{\theta_2(S)}{T_1(S)} = \frac{r_1 r_2 K/J_2}{J_1 S^2 (S^2 + 2\zeta_{12}\,\omega_{n12}\,S + \omega_{n12}{}^2)}$$

Resonance characteristics for the transport under study have been derived. The associated damping factor, ζ, is elusive and best determined empirically at the system level.

APPENDIX III

REFERENCE OSCILLATOR ANALYSIS (Refer to Figure 14)

The regeneration time is given by the following conditions:

$$V_1 - V_3 = \eta (V_1 - V_2) + V_d$$

$$V_3 = V_1 e^{-tr/\tau}$$

Where

η = the intrinsic standoff ratio = .6

τ = $C_1 (R_1 + R_4)$

V_d = forward B1 to emitter voltage drop = .5 volts

t_r = regeneration time and time is measured from the beginning of a regenerative transition.

V_2 is given by the equation

$$V_2 = V_{be3} \left(1 + \frac{R_3}{R_2}\right)$$

From the above equations

$$V_3 = V_1 e^{-tr/\tau} = V_1 (1 - \eta) + \eta V_{be3} \left(1 + \frac{R_3}{R_2}\right) - V_d$$

Or

$$t_r = \tau \text{ Ln } \frac{V_1}{V_1 (1 - \eta) + \eta V_{be3} \left(1 + \frac{R_3}{R_2}\right) - V_d}$$

The dominant term of the above equation is $V_1 (1 - \eta)$, therefore, the oscillator period is given approximately by

$$t_r \approx \tau \text{ Ln } \frac{V_1}{V_1 (1 - \eta)} = \tau (0.92)$$

Or the oscillation frequency is

$$f = \frac{1}{t_r} \approx \frac{1.1}{\tau}$$

Clearly, the ratio R_3/R_2 could be chosen such that

$$\eta V_{be3} (1 + \frac{R_3}{R_2}) - V_d = 0$$

Or

$$\frac{R_3}{R_2} = \frac{V_d}{V_{be3}} \frac{1}{\eta} - 1$$

For these conditions, the expression given above for oscillation frequency would be exact. Since the dominant temperature sensitive parameter of a UJT oscillator is the forward voltage drop, V_d, it would be desirable to also match the temperature coefficient of the junction voltage V_{be3} to the coefficient of V_d. However, in order to achieve the stability requirements of the subject system, the temperature sensitivity of the components making up the time constant τ must also be compensated. The first order effects of the temperature coefficient of V_{be3} may be evaluated by finding the partial derivative of t_r with respect to V_{be3}.

$$\frac{\partial t_r}{\partial V_{be3}} = \frac{-\tau\eta (1 + \frac{R_3}{R_2})}{V_1 (1 - \eta) + \eta V_{be3} (1 + \frac{R_3}{R_2}) - V_d} \approx \frac{-\tau (1 + \frac{R_3}{R_2})\eta}{V_1 (1 - \eta)}$$

Similarly,

$$\frac{\partial t_r}{\partial V_d} = \frac{\tau}{V_1 (1 - \eta) + \eta V_{be3} (1 + \frac{R_3}{R_2}) - V_d} \approx \frac{\tau}{V_1 (1 - \eta)}$$

$$\frac{\partial t_r}{\partial \tau} = \text{Ln} \frac{V_1}{V_1 (1 - \eta) + \eta V_{be3} (1 + \frac{R_3}{R_2}) - V_d} \approx .92$$

The total variation of the regeneration time may be expressed as

$$\Delta t_r = \frac{\partial t_r}{\partial \tau}\,\Delta\tau + \frac{\partial t_r}{\partial V_d}\,\Delta V_d + \frac{\partial t_r}{\partial V_{be3}}\,\Delta V_{be3}$$

If the parameter variations are linear temperature effects, i.e.,

$$\Delta\tau = \tau\, K_\tau\, \Delta T$$

$$\Delta V_d = V_d\, K_{V_d}\, \Delta T$$

$$\Delta V_{be3} = V_{be3}\, K_{V_{be3}}\, \Delta T$$

Where K_τ, K_{V_d}, and $K_{V_{be3}}$ are temperature coefficients, and ΔT is the temperature variation from ambient. Equating Δt_r to zero and substituting partial derivative expressions yields the first order expression,

$$.92\,\tau K_\tau + \frac{\tau}{V_1(1-\beta)}\,V_d\,K_{V_d} - \frac{\tau\left(1+\frac{R_3}{R_2}\right)\beta\,V_{be3}\,K_{V_{be3}}}{V_1(1-\beta)} = 0$$

Or

$$\frac{R_3}{R_2} = \frac{(.92\,K_\tau V_1(1-\beta) + V_d\,K_{Vd})}{\beta\,K_{V_{be3}}\,V_{be3}} - 1$$

The above expression gives the ratio R_3/R_2 required for an overall oscillator first order temperature coefficient of zero. In practice, lack of knowledge of the parameter temperature coefficients forces one to temperature cycle the oscillator and trim the ratio R_3/R_2 to obtain satisfactory temperature stability. R_1 may be adjusted for the desired frequency and readjusted after obtaining the final setting of R_3.